

The Supplementary Information for

**Efficient Luminescent Properties and Cation
Recognition Ability of Heavy Group 13 Element
Complexes of N₂O₂- and N₂O₄-Type Dipyrrins**

Akinobu Sumiyoshi, Yusuke Chiba, Ryota Matsuoka, Takumu Noda and Tatsuya Nabeshima*

Graduate School of Pure and Applied Sciences
and Tsukuba Research Center for Energy Materials Science (TREMS),
University of Tsukuba, 1-1-1 Tennodai, Tsukuba, Ibaraki 305-8571, Japan

*Corresponding Author. Email: nabesima@chem.tsukuba.ac.jp

Table of Contents

Characterization of the compounds.....	3
UV-vis absorption/emission measurements	14
Computational studies.....	18
Time-resolved fluorescence analyses	19
Ion sensing study	22
X-ray crystallographic analyses.....	40
References for the Supporting Information	43

Characterization of the compounds

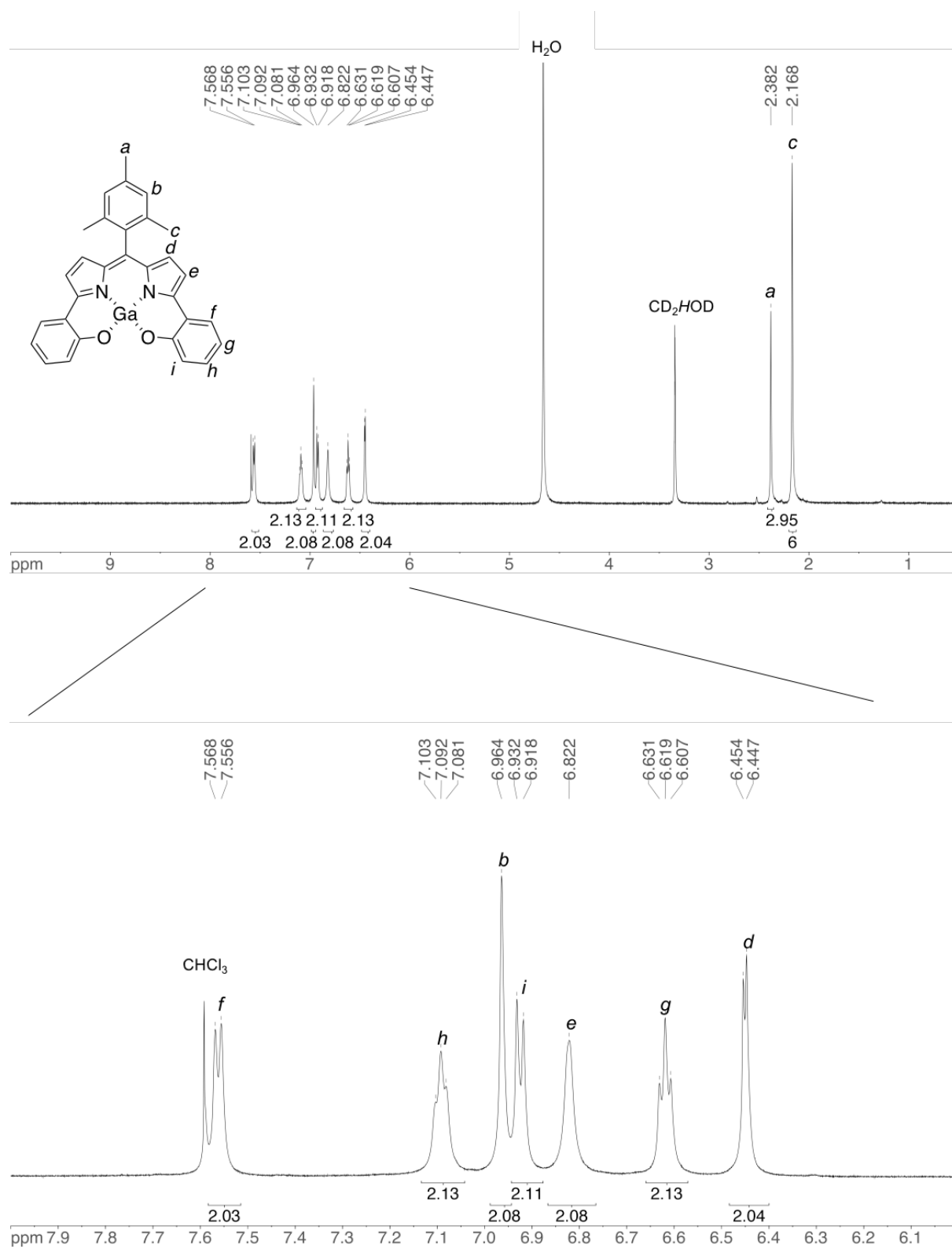


Figure S1 ^1H NMR spectrum of $[\text{L1Ga}(\text{L}')_2]$ (600 MHz, $\text{CDCl}_3/\text{CD}_3\text{OD}$ = 1/1 (v/v)).

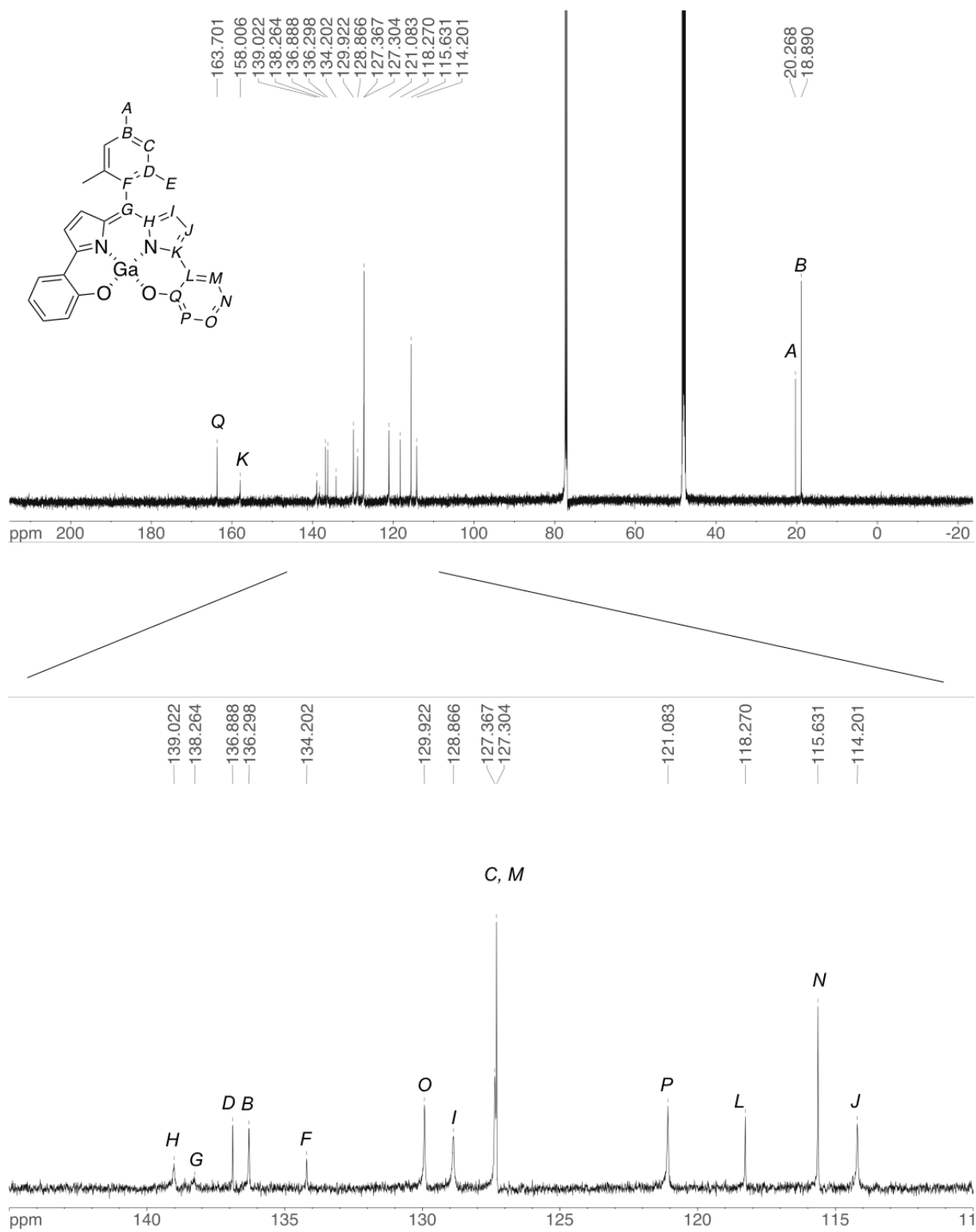


Figure S2 ¹³C NMR spectrum of [L1Ga(L')₂] (151 MHz, CDCl₃/CD₃OD = 1/1 (v/v)).

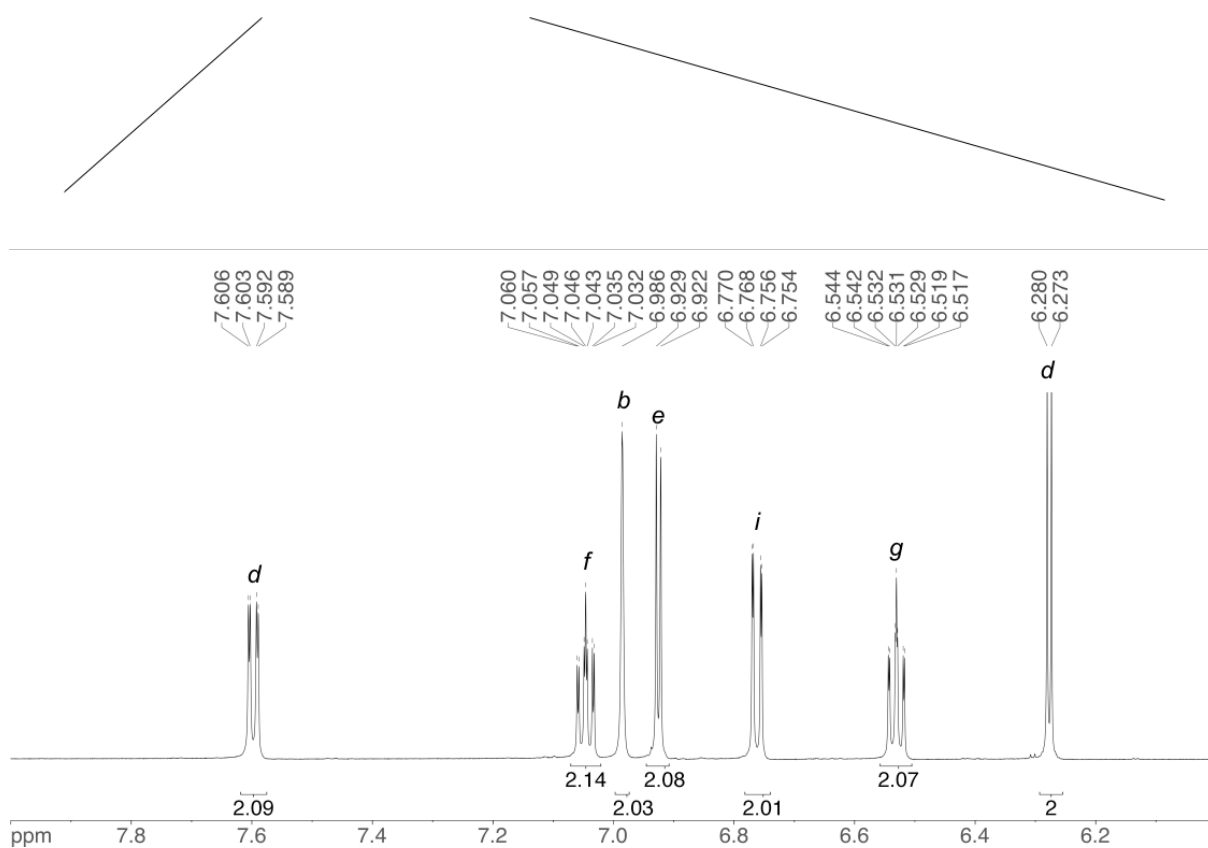
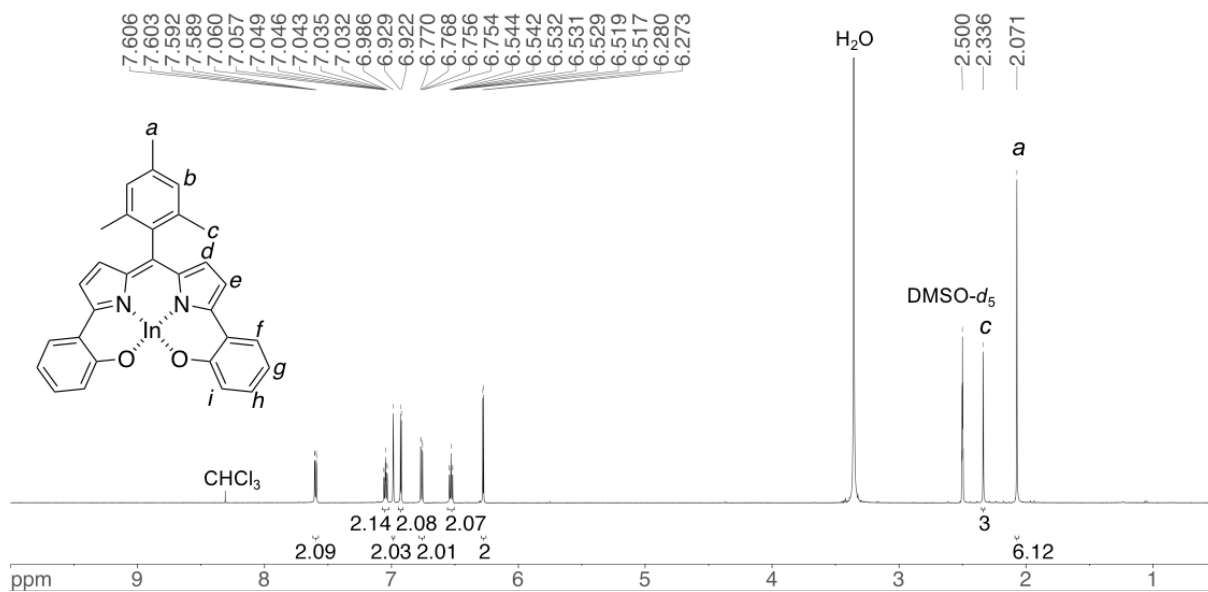


Figure S3 1H NMR spectrum of $[L1In(L')_2]$ (600 MHz, $DMSO-d_6$).

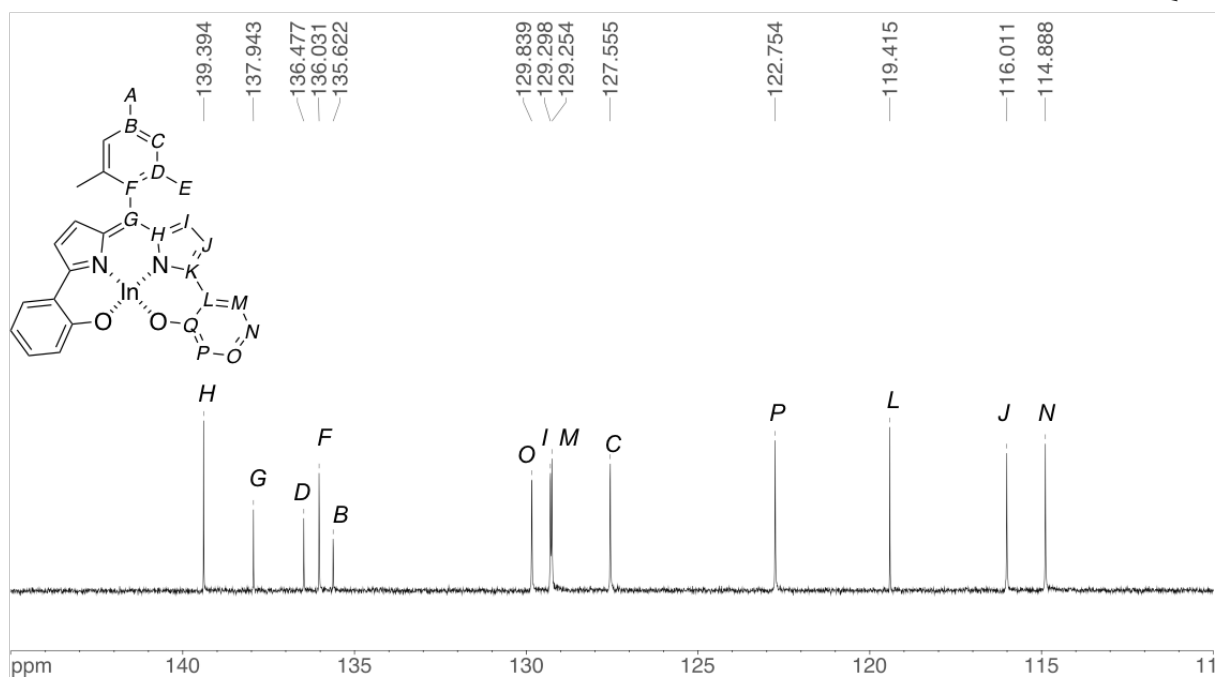
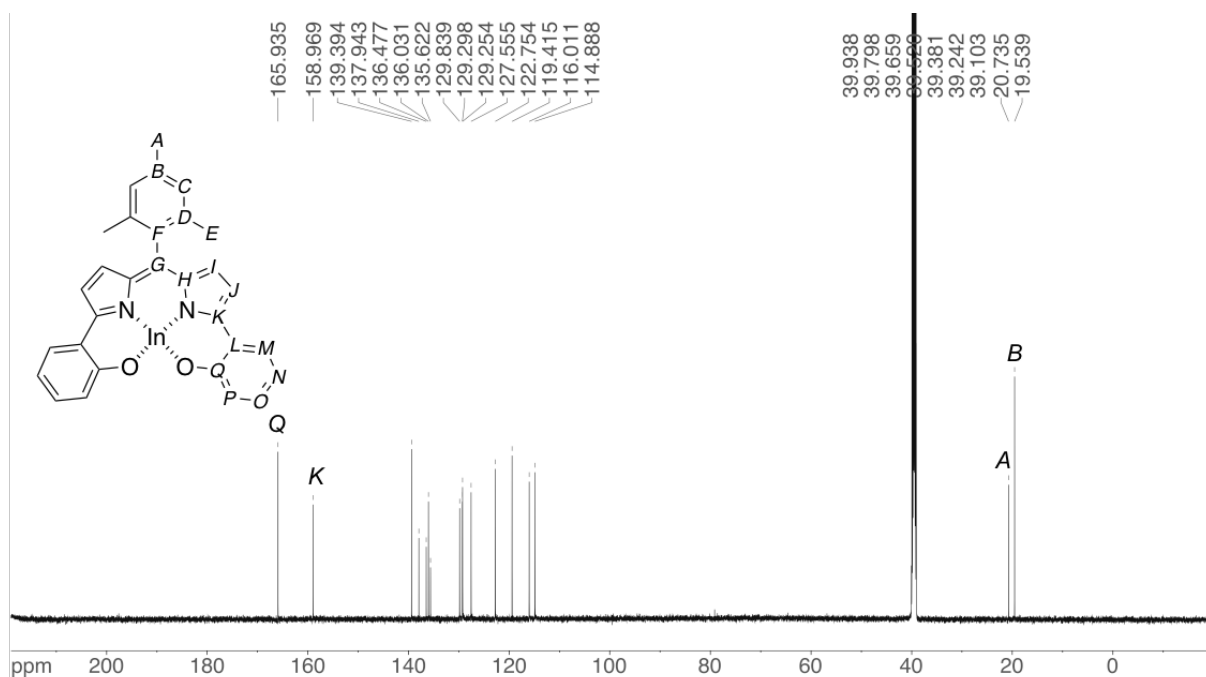


Figure S4 ^{13}C NMR spectrum of $[\text{L1In}(\text{L}')_2]$ (151 MHz, $\text{DMSO-}d_6$).

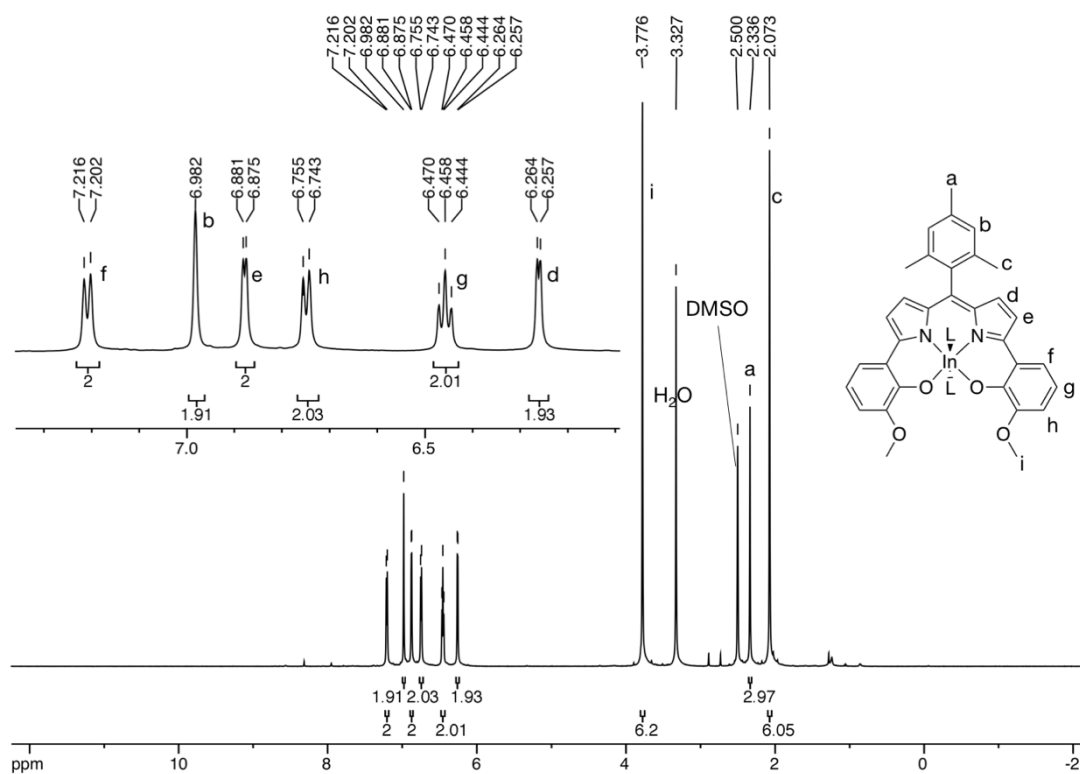


Figure S5 1H NMR spectrum of $[L_2In(L')_2]$ (600 MHz, DMSO- d_6).

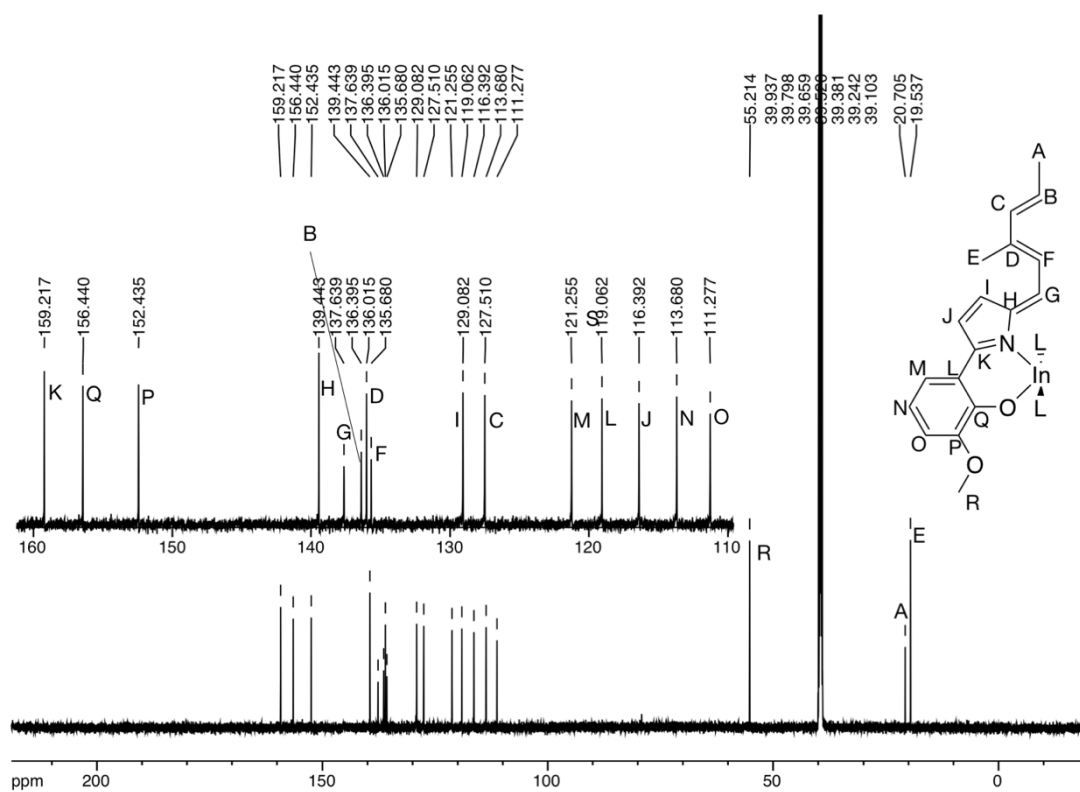


Figure S6 ^{13}C NMR spectrum of $[L_2In(L')_2]$ (151 MHz, DMSO- d_6).

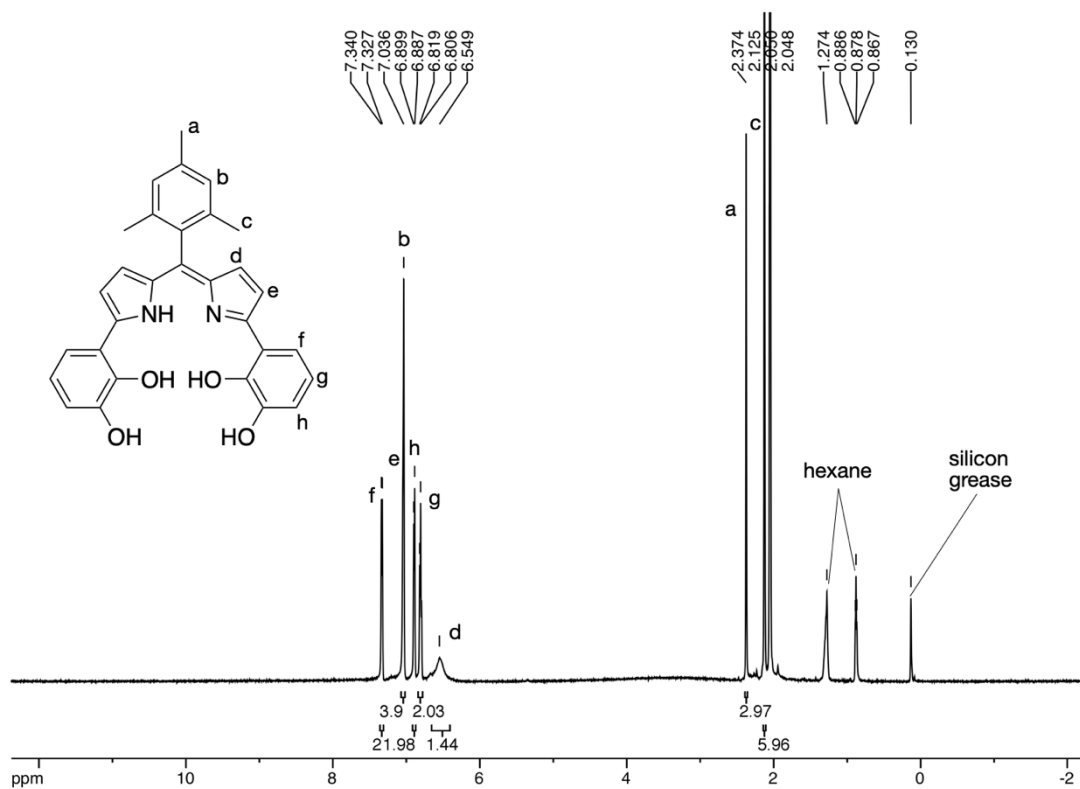


Figure S7 ^1H NMR spectrum of H_3L_3 (400 MHz, acetone- d_6).

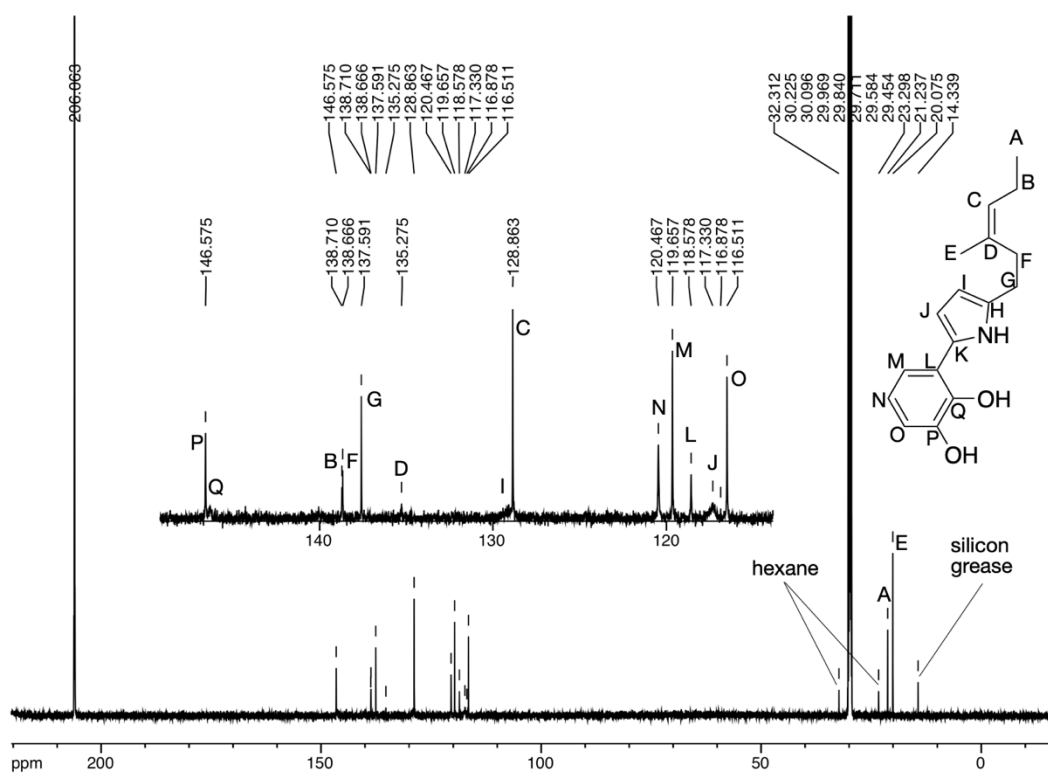


Figure S8 ^{13}C NMR spectrum of H_3L_3 (101 MHz, acetone- d_6).

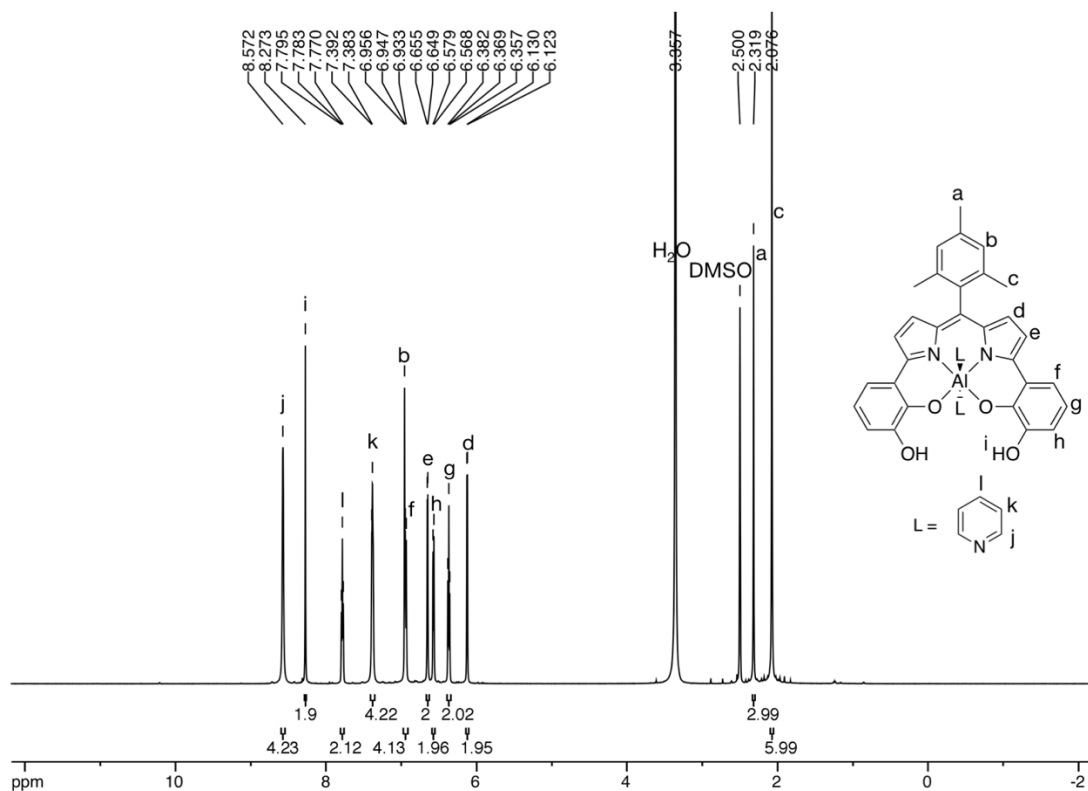


Figure S9 1H NMR spectrum of $[L_3Al(L')_2]$ (L' : solvent and/or pyridine) (600 MHz, $DMSO-d_6$).

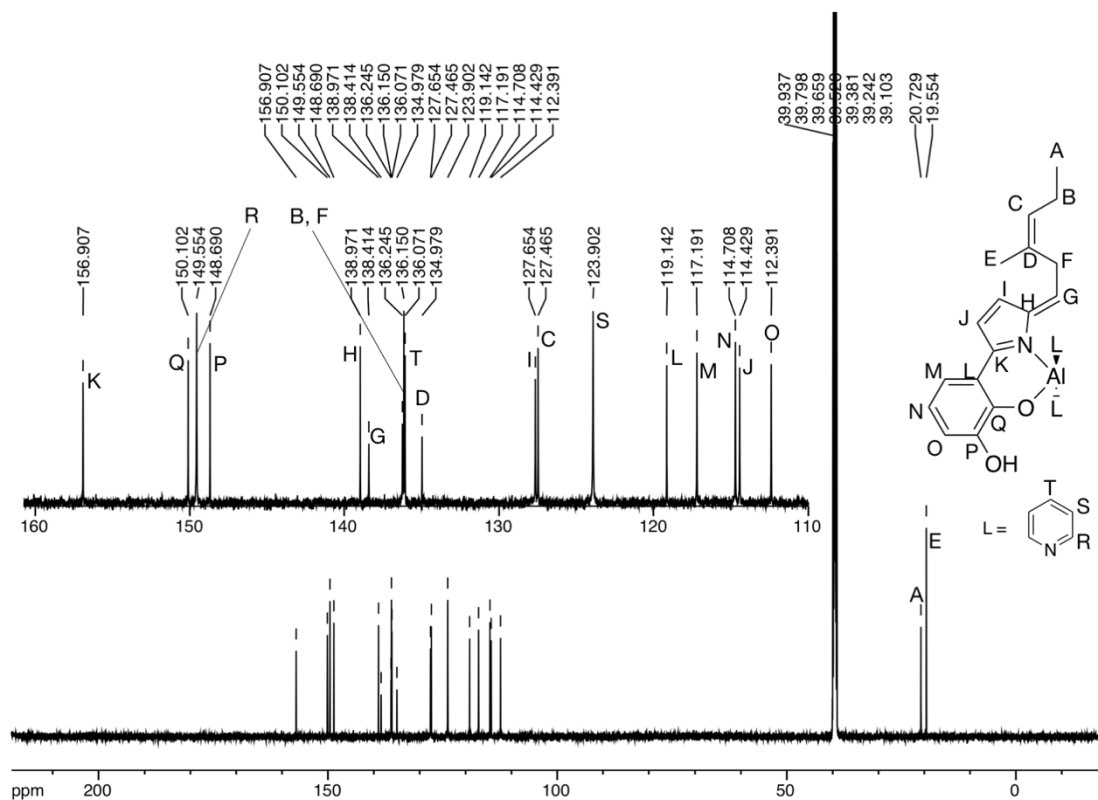


Figure S10 ^{13}C NMR spectrum of $[L_3Al(L')_2]$ (L' : solvent and/or pyridine) (151 MHz, $DMSO-d_6$).

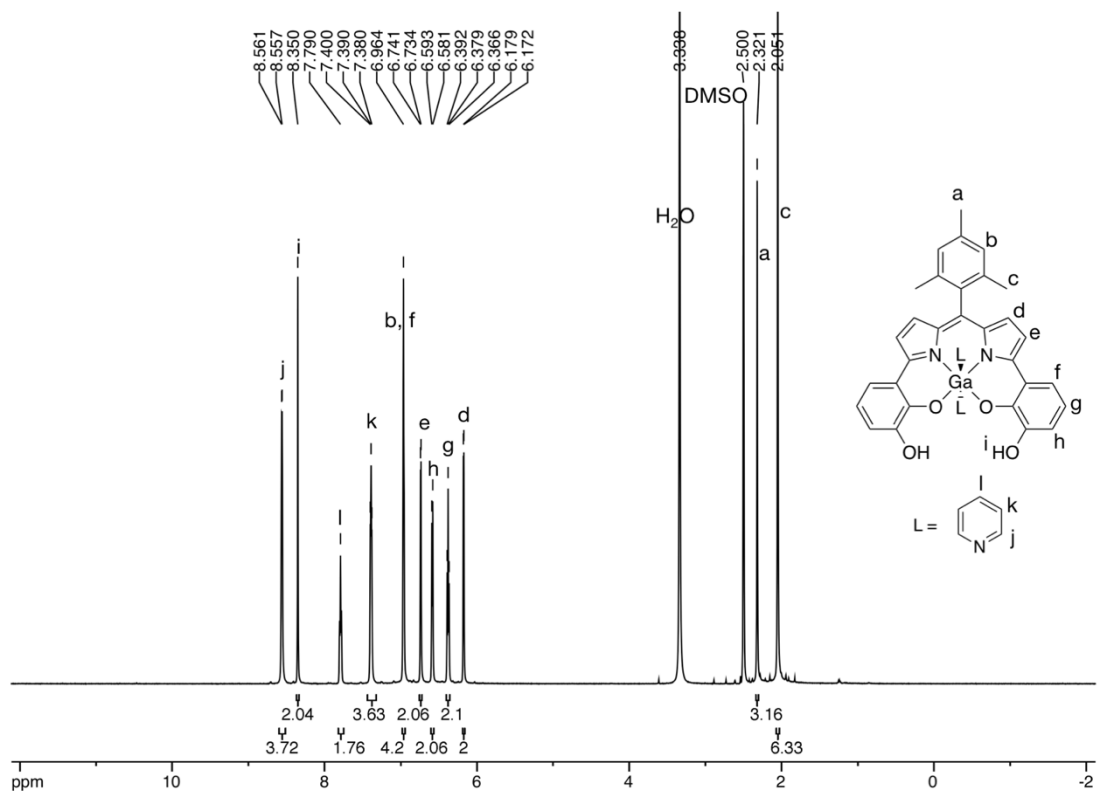


Figure S11 1H NMR spectrum of $[L_3Ga(L')_2]$ (L' : solvent and/or pyridine) (600 MHz, $DMSO-d_6$).

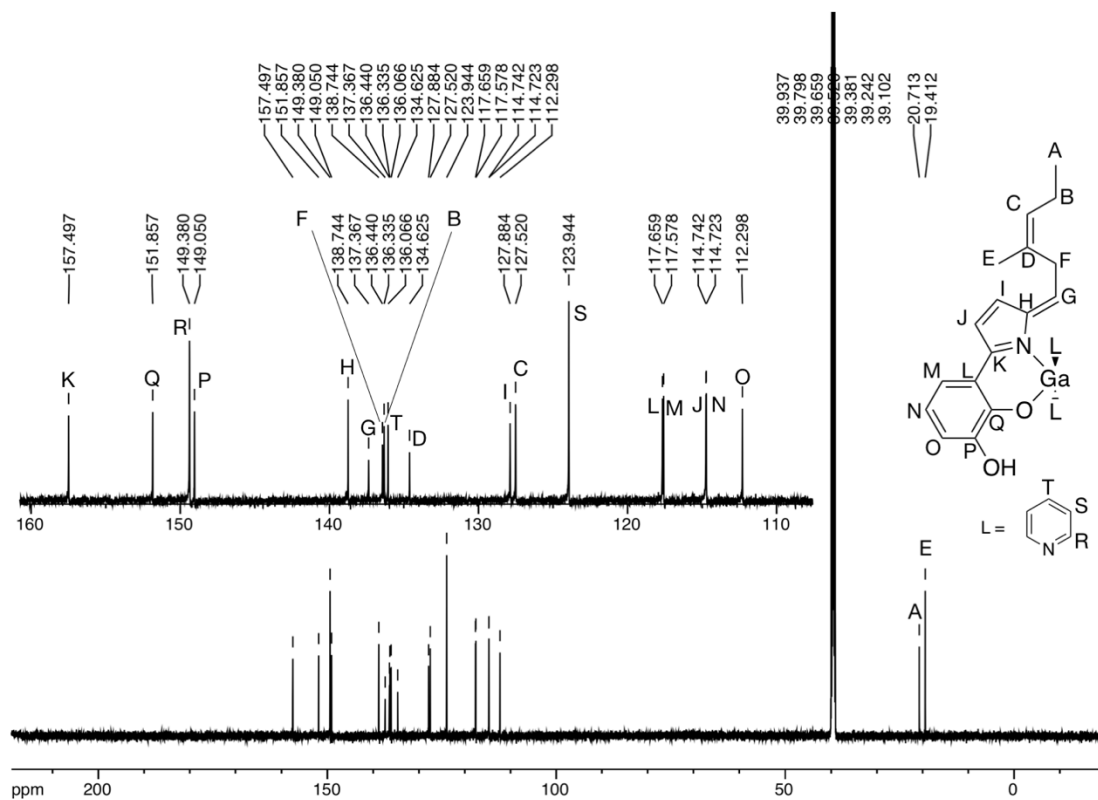


Figure S12 ^{13}C NMR spectrum of $[L_3Ga(L')_2]$ (L' : solvent and/or pyridine) (151 MHz, $DMSO-d_6$).

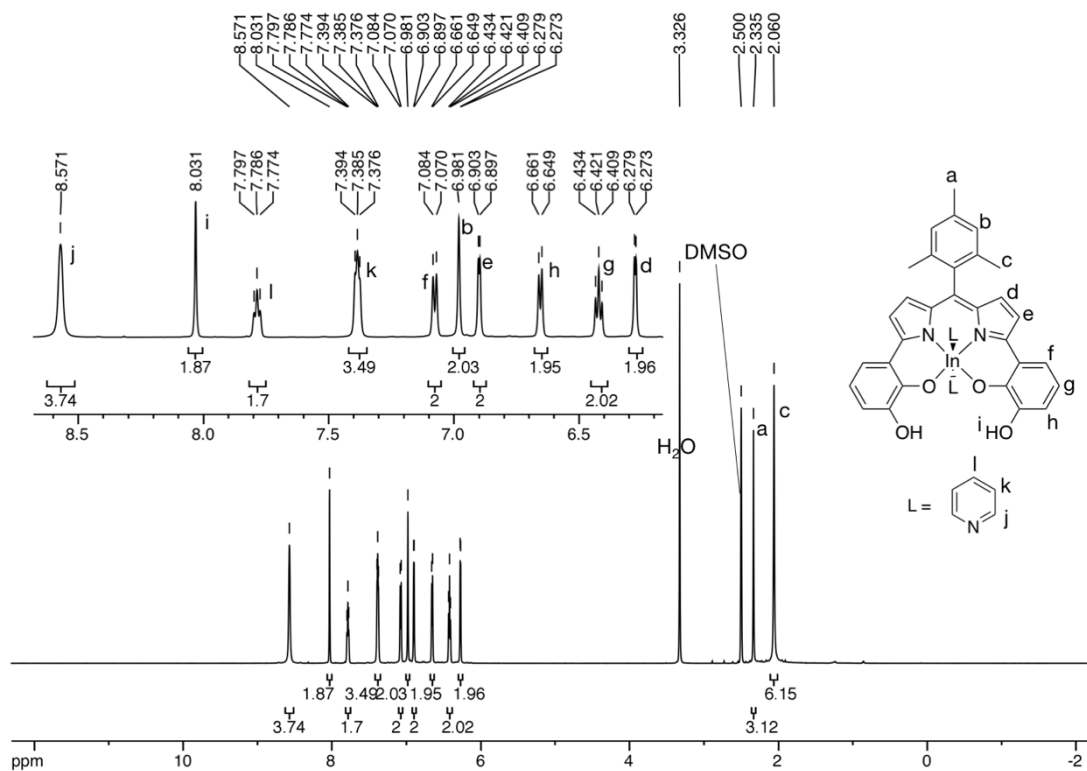


Figure S13 1H NMR spectrum of $[L_3In(L')_2]$ (L' : solvent and/or pyridine) (600 MHz, $DMSO-d_6$).

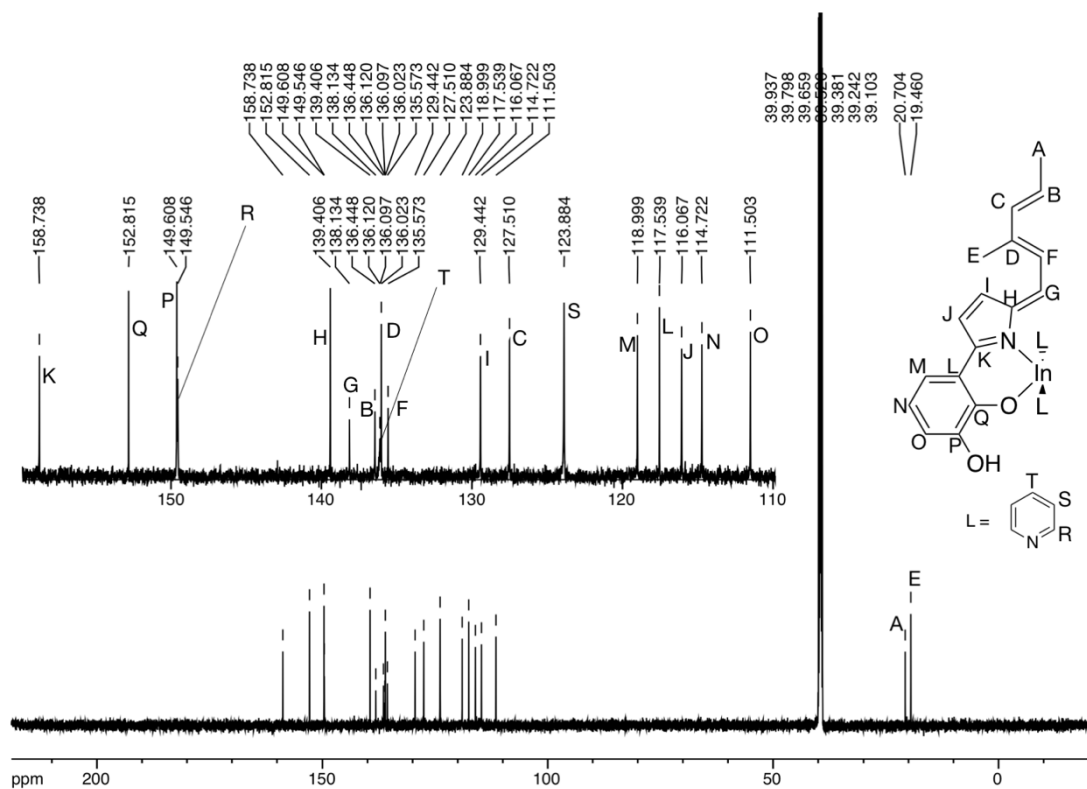


Figure S14 ^{13}C NMR spectrum of $[L_3In(L')_2]$ (L' : solvent and/or pyridine) (151 MHz, $DMSO-d_6$).

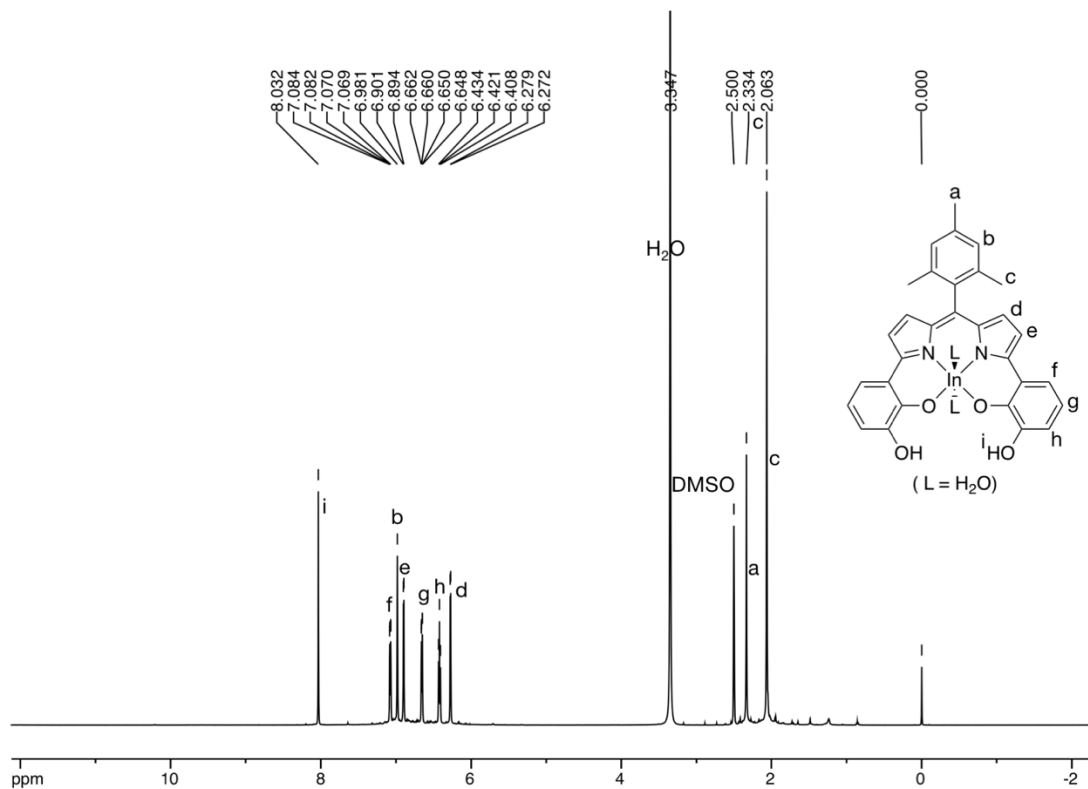


Figure S15 1H NMR spectrum of $[L_3In(L')_2]$ (600 MHz, DMSO-*d*₆).

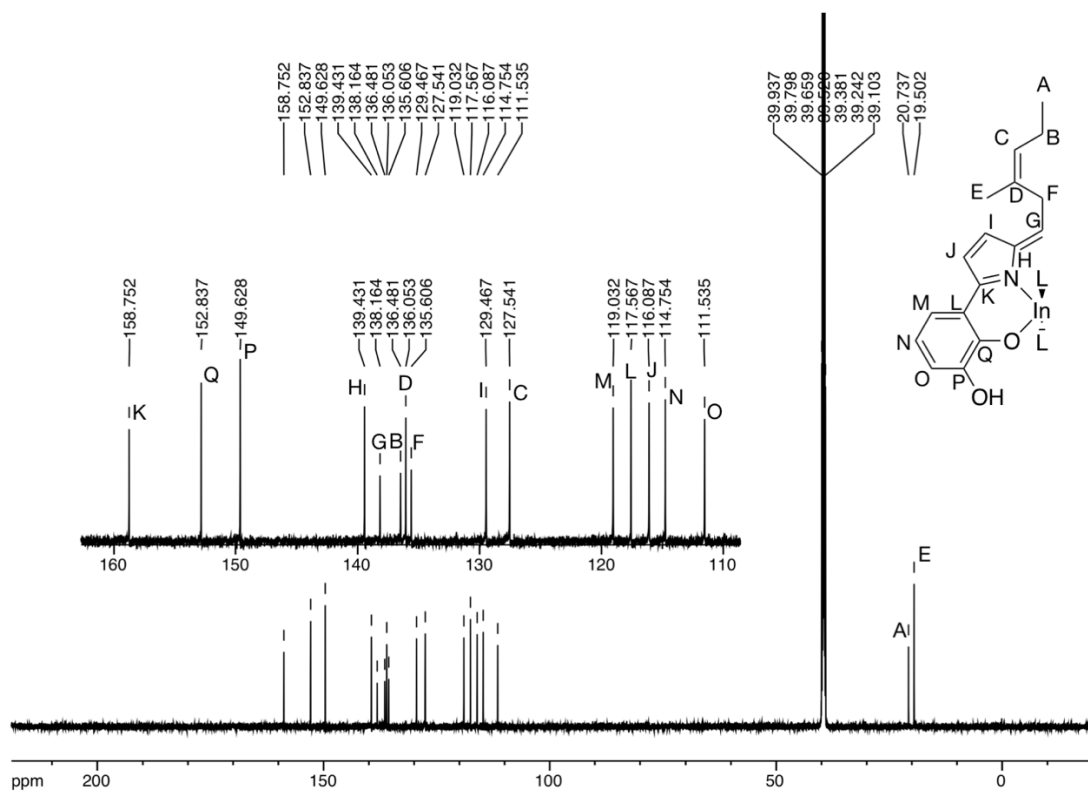


Figure S16 ^{13}C NMR spectrum of $[L_3In(L')_2]$ (151 MHz, DMSO-*d*₆).

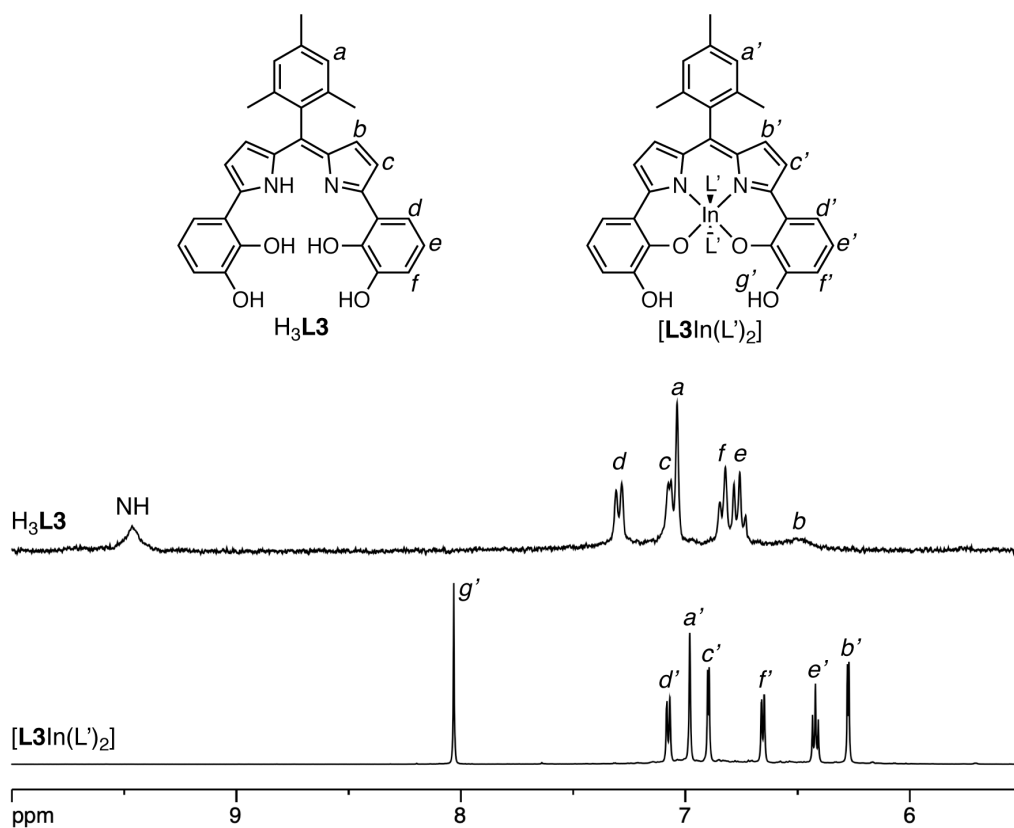


Figure S17. ^1H NMR spectra of $\text{H}_3\text{L3}$ (top) and $[\text{L3In}(\text{L}')_2]$ (bottom) (400 MHz, $\text{DMSO-}d_6$, 298 K, $\text{L}' = \text{solvent}$).

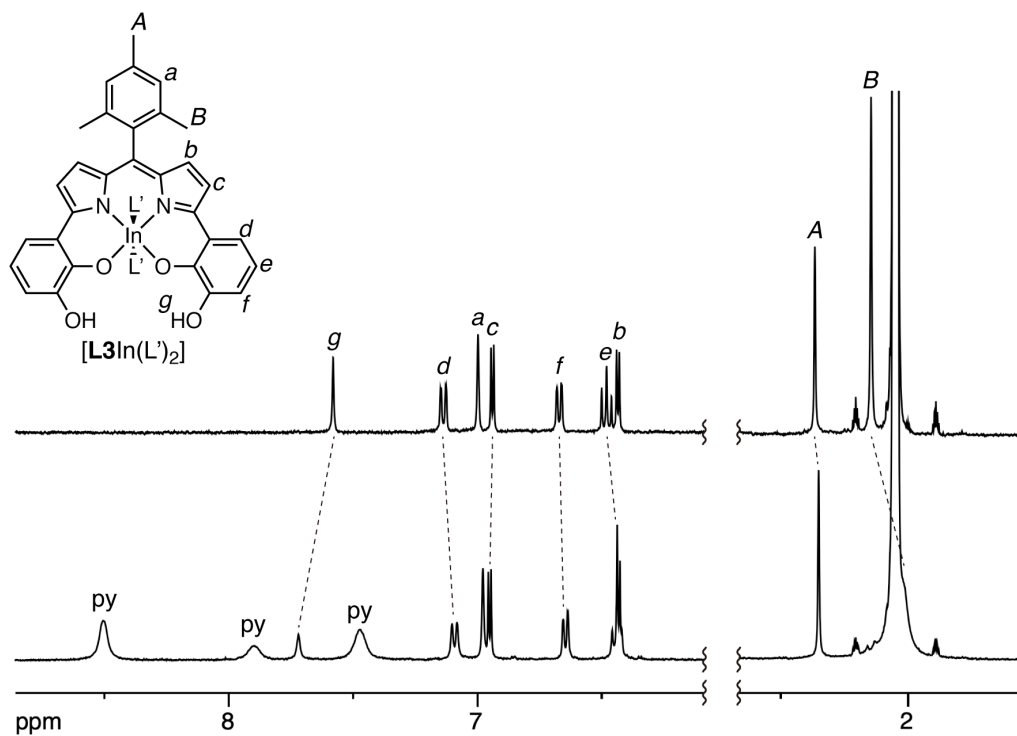


Figure S18. ^1H NMR spectra of $[\text{L3In}(\text{L}')_2]$ with 1.6 eq. of pyridine (bottom) and that without pyridine (top) (400 MHz, $\text{acetone-}d_6$, 298 K).

UV-vis absorption/emission measurements

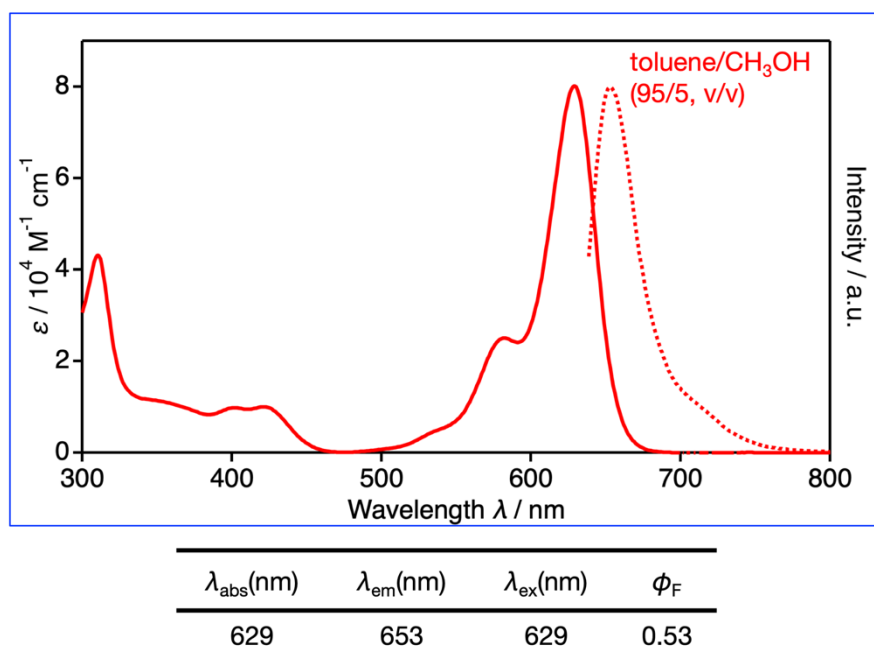


Figure S19 (top) UV-vis absorption (solid line) and emission (dotted line) spectra of [L1Ga(L')₂] (L': solvent) (toluene/CH₃OH = 95/5 (v/v), 10 μ M, 293 K). (bottom) Optical properties of the complex.

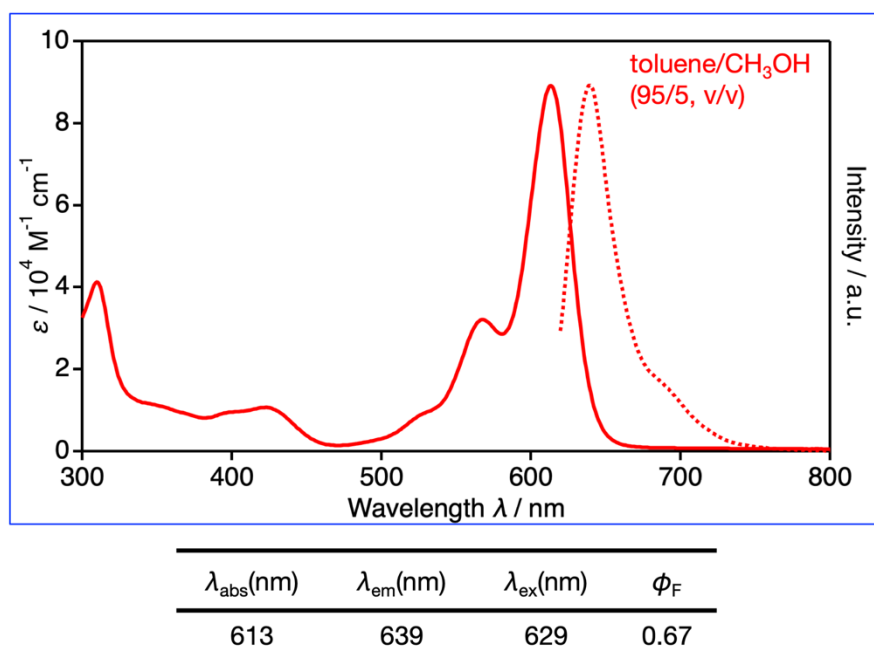


Figure S20 (top) UV-vis absorption (solid line) and emission (dotted line) spectra of [L1In(L')₂] (L': solvent) (toluene/CH₃OH = 95/5 (v/v), 10 μ M, 293 K). (bottom) Optical properties of the complex.

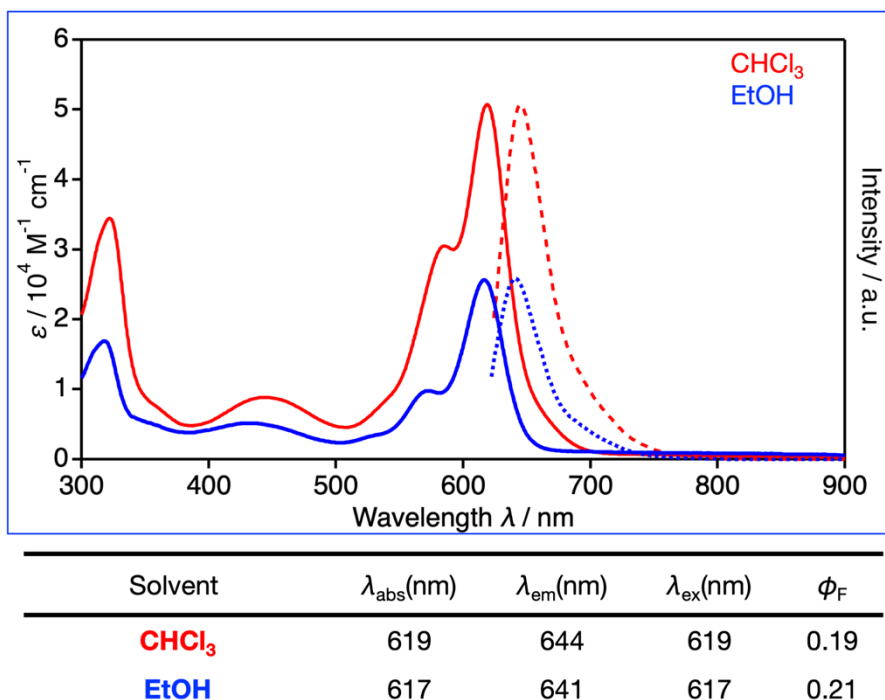


Figure S21 (top) UV-vis absorption (solid line) and emission (dotted line) spectra of $[\text{L2In}(\text{L}')_2]$ (L' : solvent) in various solvents (10 μM , 293 K). (bottom) Optical properties of the complex.

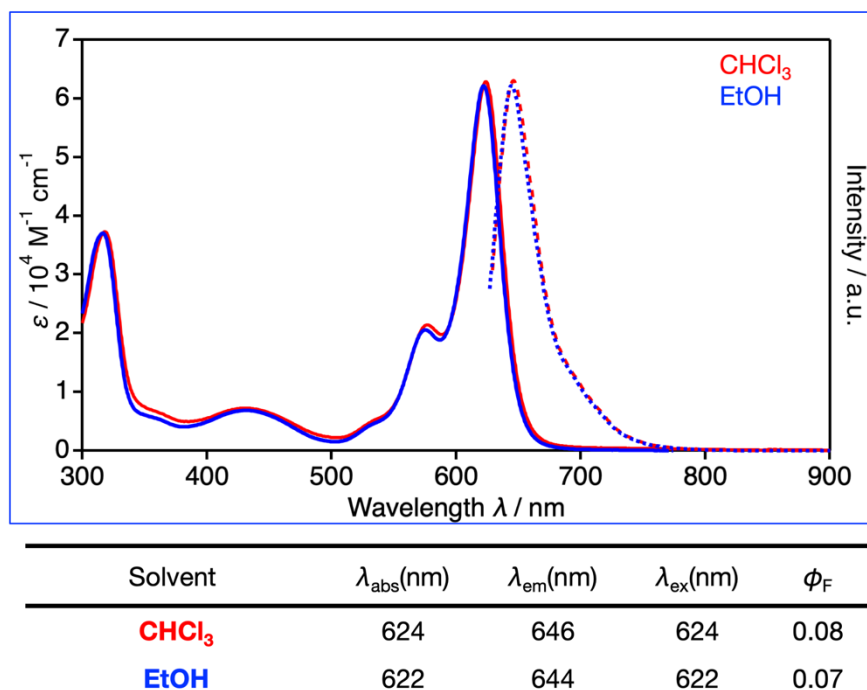


Figure S22 (top) UV-vis absorption (solid line) and emission (dotted line) spectra of $[\text{L3Al}(\text{L}')_2]$ (L' : solvent and/or pyridine) in various solvents (10 μM , 293 K). (bottom) Optical properties of the complex.

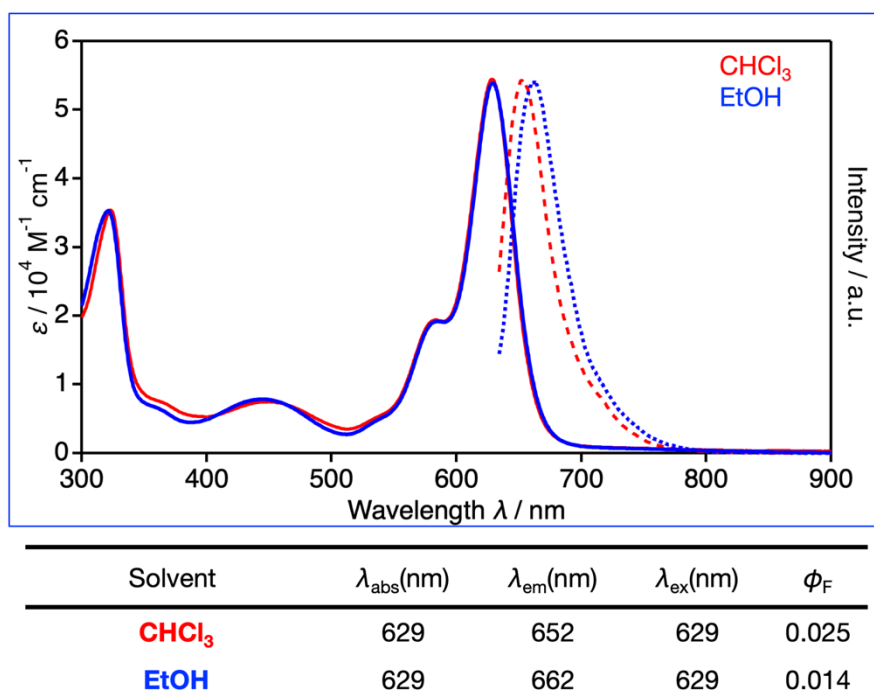


Figure S23 (top) UV-vis absorption (solid line) and emission (dotted line) spectra of $[\text{L3Ga}(\text{L}')_2]$ (L' : solvent and/or pyridine) in various solvents (10 μM , 293 K). (bottom) Optical properties of the complex.

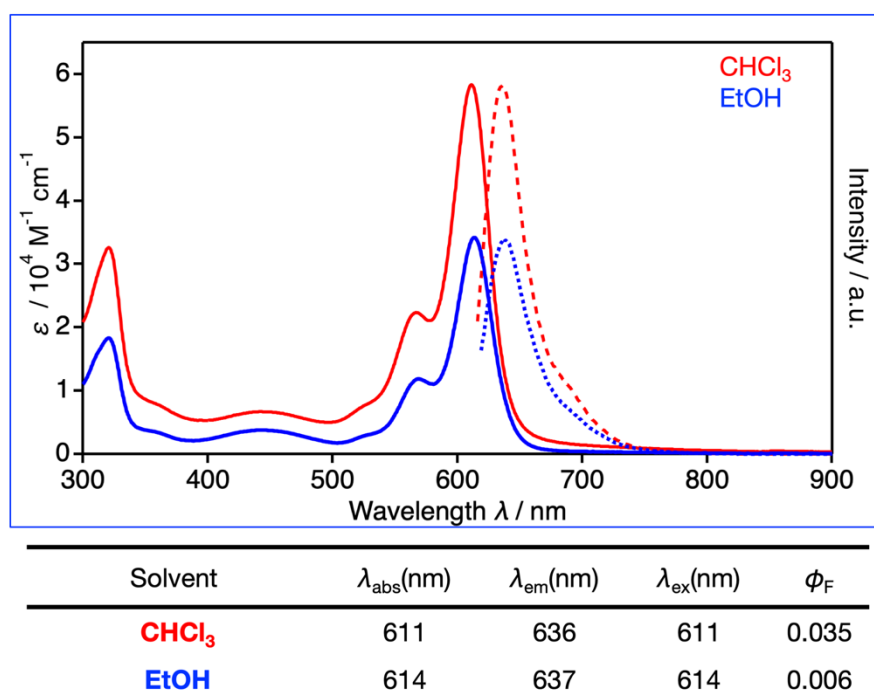
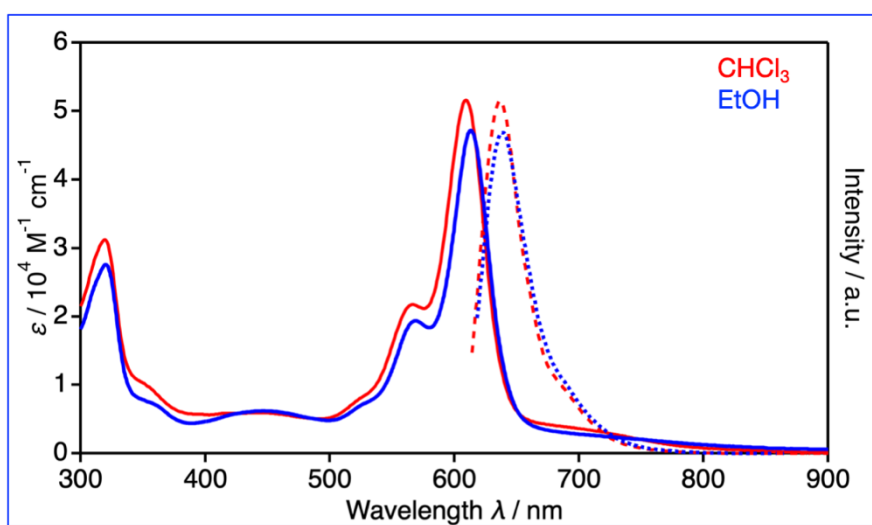


Figure S24 (top) UV-vis absorption (solid line) and emission (dotted line) spectra of $[\text{L3In}(\text{L}')_2]$ (L' : solvent and/or pyridine) in various solvents (10 μM , 293 K). (bottom) Optical properties of the complex.



Solvent	$\lambda_{\text{abs}}(\text{nm})$	$\lambda_{\text{em}}(\text{nm})$	$\lambda_{\text{ex}}(\text{nm})$	ϕ_{F}
CHCl₃	609	636	609	0.015
EtOH	613	639	613	0.004

Figure S25 (top) UV-vis absorption (solid line) and emission (dotted line) spectra of $[\text{L3In}(\text{L}')_2]$ (L' : solvent) in various solvents ($10 \mu\text{M}$, 293 K). (bottom) Optical properties of the complex.

Computational studies

DFT and TD-DFT calculations on the model compound [**L2**In(MeOH)₂] were conducted using the B3LYP functional with the 6-31+G* (for C, H, N, and O) and LANL2DZ (for In) basis sets. The geometry optimized structure and Kohn-Sham frontier orbitals of the complex was shown in **Figure S26** below. Although the HOMO and LUMO distribute over the entire conjugated π -system of the N₂O₄ dipyrin unit, the indium center has no contribution to these orbitals. The lowest-energy absorption band of this complex was assigned by the TD-DFT calculation to the ¹ π - π^* (HOMO \rightarrow LUMO) transition of the N₂O₄ dipyrin unit. These results suggest that the central metal ion should have little electronic contribution to the optical properties of the N₂O₄ dipyrin complexes.

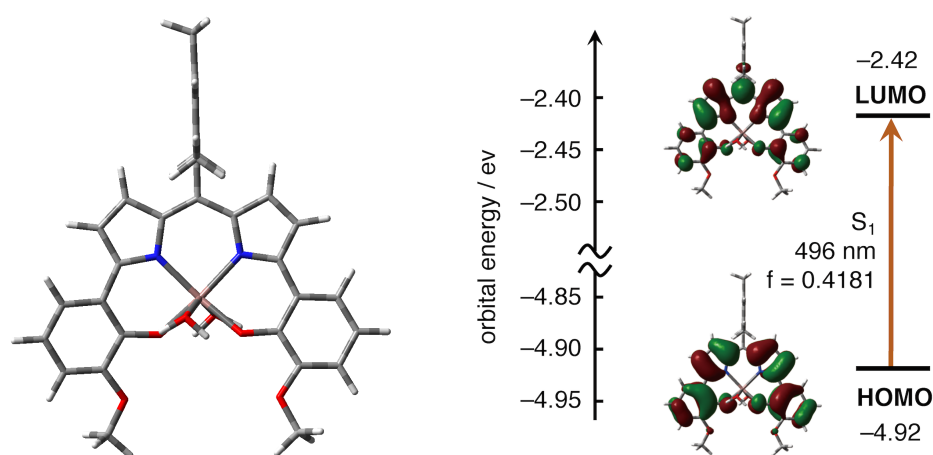


Figure S26 Geometry-optimized structure (left) and Kohn-Sham frontier orbitals (right) of [**L2**In(MeOH)₂] obtained by DFT calculations at the B3LYP/6-31+G* (for C, H, N, and O) and B3LYP/LANL2DZ (for In) level. The vertical transition energies of the complexes calculated by the TD-DFT calculations at the same level are also shown in the right figure.

Time-resolved fluorescence analyses

Fluorescence lifetime measurements were carried out on a time correlated single photon counting (TCSPC) setup using Fluorolog-3, Horiba. All samples were excited at 634 nm, employing a light emitting diode laser (NanoLED-635L, Peak wavelength: 634 nm, Pulse duration: <200 ps) as a light source. The obtained data were fitted by using the Horiba DAS6 software.

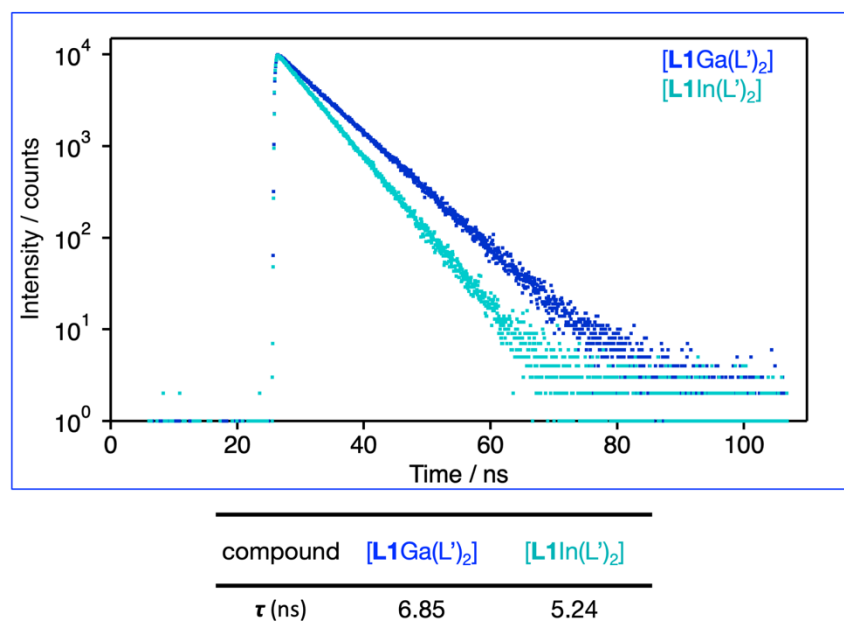
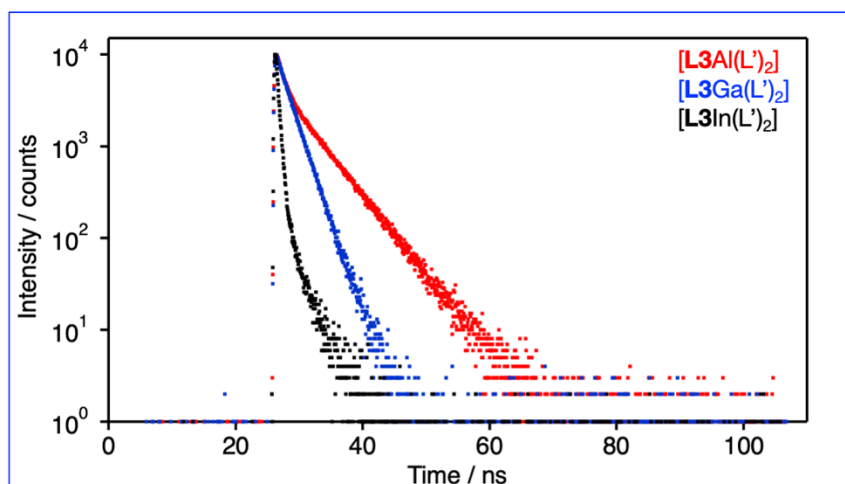
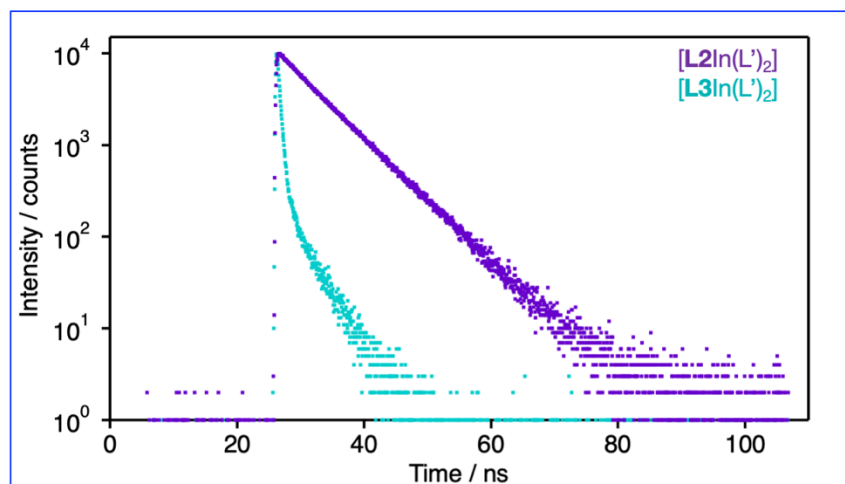


Figure S27 (top) Fluorescence time decay curves of [L1Ga(L')₂] (L': solvent) and [L1In(L')₂] (L': solvent) (toluene/CH₃OH = 95/5 (v/v), 10 μ M, 298 K). (bottom) The determined fluorescence lifetimes of the complexes.



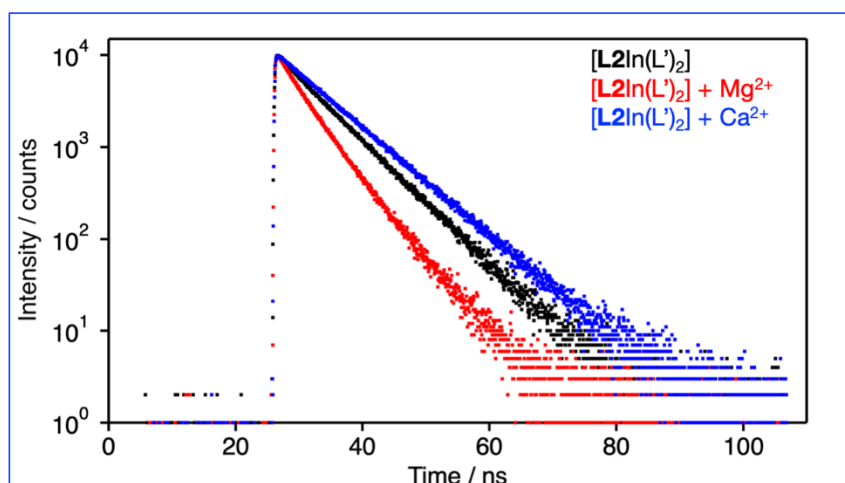
compound	[L3Al(L') ₂]	[L3Ga(L') ₂]	[L3In(L') ₂]
τ_1 (ns)	1.02 (26%)	2.06	0.407 (92%)
τ_2 (ns)	4.97 (74%)	–	2.23 (8%)

Figure S28 (top) Fluorescence time decay curves of [L3Al(L')₂], [L3Ga(L')₂], and [L3In(L')₂] (CHCl₃/CH₃OH = 9/1 (v/v), 10 μ M, 298 K, L': solvent and/or pyridine). (bottom) The determined fluorescence lifetimes of the complexes.



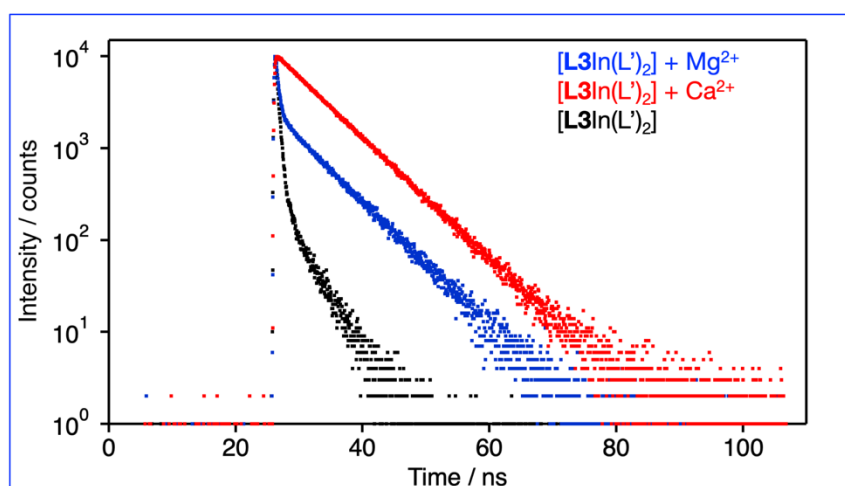
compound	[L2In(L') ₂]	[L3In(L') ₂]
τ_1 (ns)	3.40 (6%)	0.425 (83%)
τ_2 (ns)	6.51 (94%)	3.25 (17%)

Figure S29 (top) Fluorescence time decay curves of [L2In(L')₂] and [L3In(L')₂] (CHCl₃/CH₃OH = 9/1 (v/v), 10 μ M, 298 K, L': solvent). (bottom) The determined fluorescence lifetimes of the complexes.



compound	[L2In(L') ₂]	[L2In(L') ₂] + Mg ²⁺	[L2In(L') ₂] + Ca ²⁺
τ ₁ (ns)	3.40 (6%)	3.23 (47%)	7.37
τ ₂ (ns)	6.51 (94%)	5.43 (53%)	–

Figure S30 (top) Fluorescence time decay curves of [L2In(L')₂] and [L2In(L')₂] with alkaline earth ions (perchlorate salt, 5.5 equiv.) (CHCl₃/CH₃OH = 9/1 (v/v), 10 μM, 298 K, L': solvent). (bottom) The determined fluorescence lifetimes of the complexes.



compound	[L3In(L') ₂]	[L3In(L') ₂] + Mg ²⁺	[L3In(L') ₂] + Ca ²⁺
τ ₁ (ns)	0.425 (83%)	0.462 (28%)	6.54
τ ₂ (ns)	3.25 (17%)	6.27 (72%)	–

Figure S31 (top) Fluorescence time decay curves of [L3In(L')₂] and [L3In(L')₂] with alkaline earth ions (perchlorate salt, 5.5 equiv.) (CHCl₃/CH₃OH = 9/1 (v/v), 10 μM, 298 K, L': solvent). (bottom) The determined fluorescence lifetimes of the complexes.

Ion sensing study

A representative procedure ($\text{Ca}(\text{ClO}_4)_2$ and $[\text{L3In}(\text{L}')_2]$)

1.06 mg of $[\text{L3In}]\cdot 2\text{H}_2\text{O}$ was dissolved in a mixed solvent of $\text{CHCl}_3/\text{EtOH} = 9/1$ (v/v) and diluted to 10 mL in a volumetric flask. 1.32 mL of this solution was then diluted to 25 mL with the same solvent in a volumetric flask to prepare a $8.9 \mu\text{M}$ stock solution of the host $[\text{L3In}(\text{L}')_2]$. 1.57 mg of $\text{Ca}(\text{ClO}_4)_2$ was dissolved in the stock solution of $[\text{L3In}(\text{L}')_2]$ and diluted to 10 mL in a volumetric flask. 1.29 mL of this solution was then diluted to 5 mL with the same stock solution in a volumetric flask to prepare a $130 \mu\text{M}$ stock solution of the guest $\text{Ca}(\text{ClO}_4)_2$. To a UV cell ($l = 1.0\text{cm}$) was added 2.50 mL of the stock solution of $[\text{L3In}(\text{L}')_2]$, and 0.02–0.30 mL each of the guest solution was titrated into the sample solution at the constant concentration of $[\text{L3In}(\text{L}')_2]$. UV-vis absorption and fluorescence measurements were performed during the titration.

For some of the host-guest complexes (Figs. S33, S35, S37, S55, S57, S59, and S61), the binding stoichiometry and association constants cannot be determined because the recognition process was complicated. For the other host-guest complexes (Figs. S38, S40, S42, S44, S46, S48, S50, S52, and S62), the association constants were determined by the least square fitting of 1:1 or 2:1 (host:guest) binding model using the TitrationFit software.^{S1}

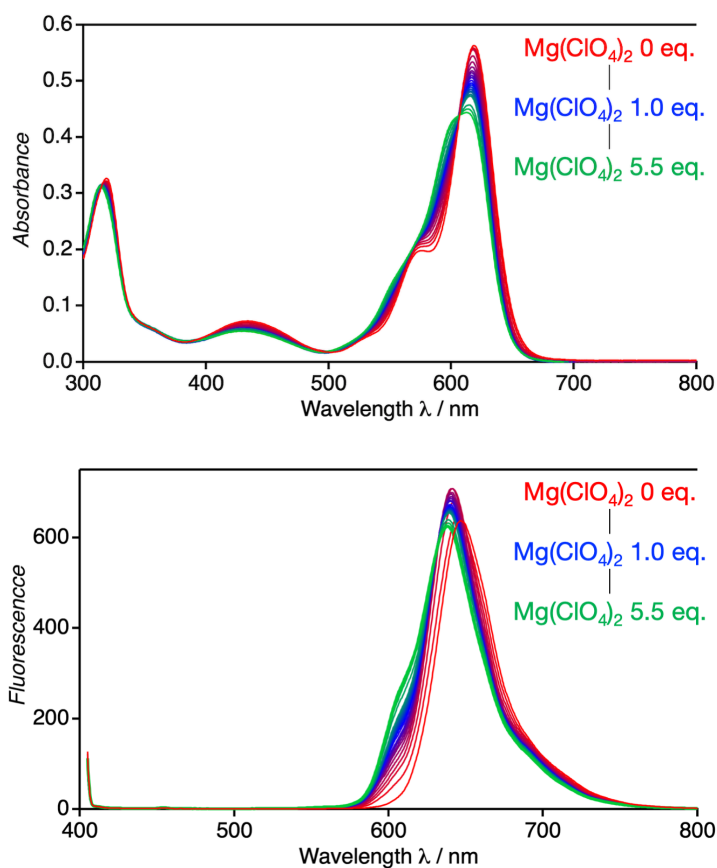


Figure S32 UV-vis absorption (top) and emission (bottom) spectral changes of $[\text{L}_2\text{In}(\text{L}')_2]$ (L' : solvent, $8.9 \mu\text{M}$) upon the addition of $\text{Mg}(\text{ClO}_4)_2$ (0–5.5 eq.) ($\text{CHCl}_3/\text{EtOH} = 9/1$ (v/v), 293 K, $\lambda_{\text{ex}} = 400$ nm).

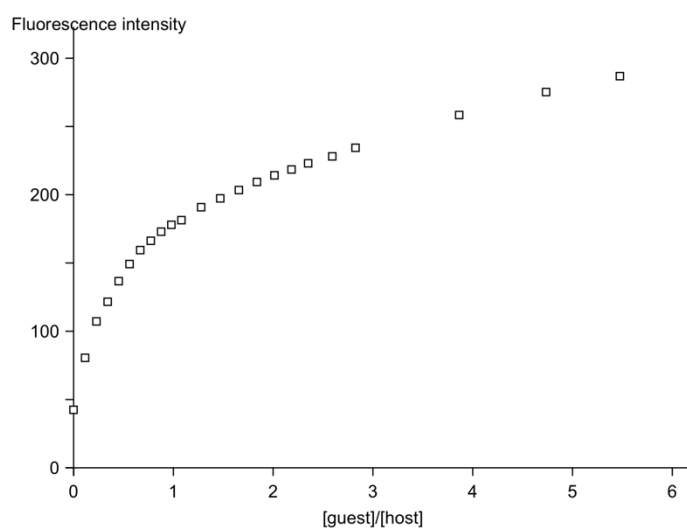


Figure S33 Changes in the emission intensity of $[\text{L}_2\text{In}(\text{L}')_2]$ ($8.9 \mu\text{M}$) at 610 nm upon the addition of $\text{Mg}(\text{ClO}_4)_2$ (0–5.5 eq.) ($\text{CHCl}_3/\text{EtOH} = 9/1$ (v/v), 293 K, $\lambda_{\text{ex}} = 400$ nm).

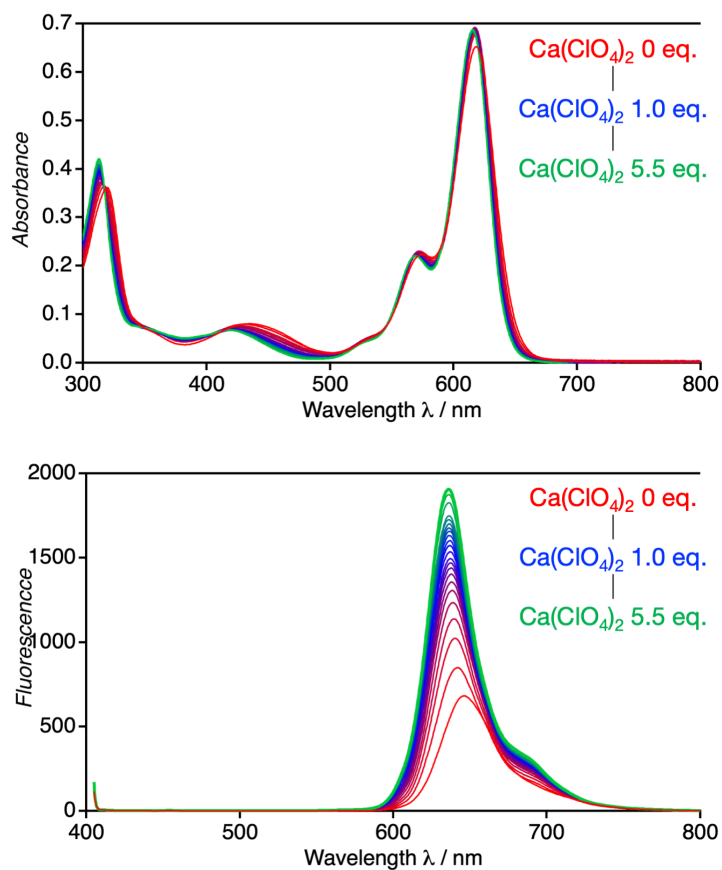


Figure S34 UV-vis absorption (top) and emission (bottom) spectral changes of [L2In(L')₂] (L': solvent, 8.9 μM) upon the addition of Ca(ClO₄)₂ (0–5.5 eq.) (CHCl₃/EtOH = 9/1 (v/v), 293 K, λ_{ex} = 400 nm).

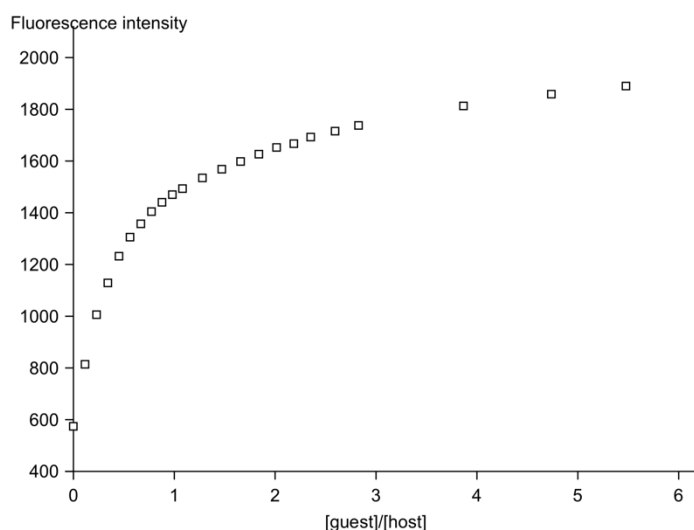


Figure S35 Changes in the emission intensity of [L2In(L')₂] (8.9 μM) at 638 nm upon the addition of Ca(ClO₄)₂ (0–5.5 eq.) (CHCl₃/EtOH = 9/1 (v/v), 293 K, λ_{ex} = 400 nm).

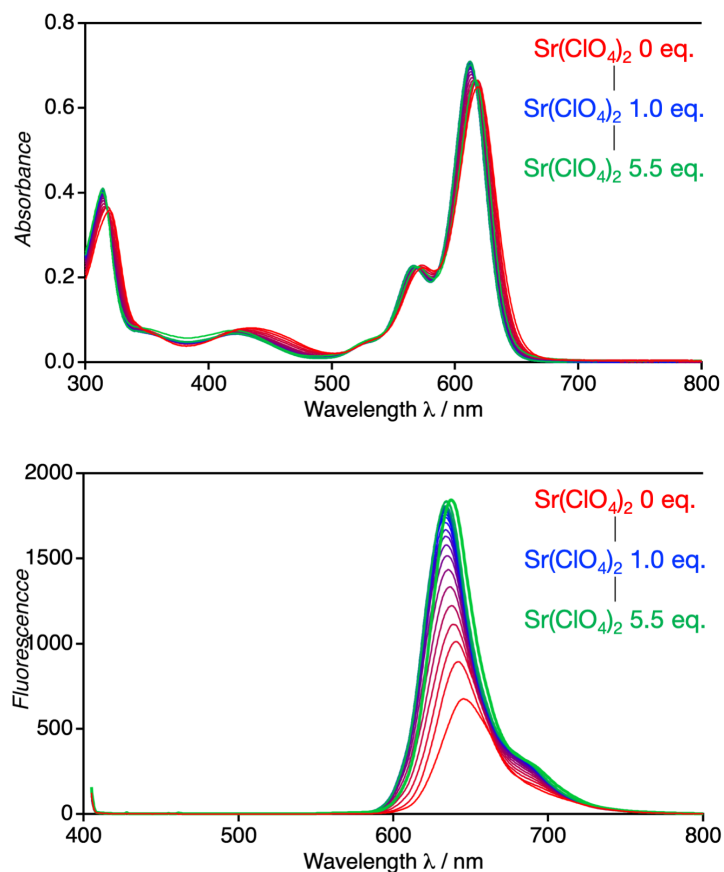


Figure S36 UV-vis absorption (top) and emission (bottom) spectral changes of [L2In(L')2] (L': solvent, 8.9 μM) upon the addition of Sr(ClO4)2 (0–5.5 eq.) (CHCl3/EtOH = 9/1 (v/v), 293 K, $\lambda_{\text{ex}} = 400$ nm).

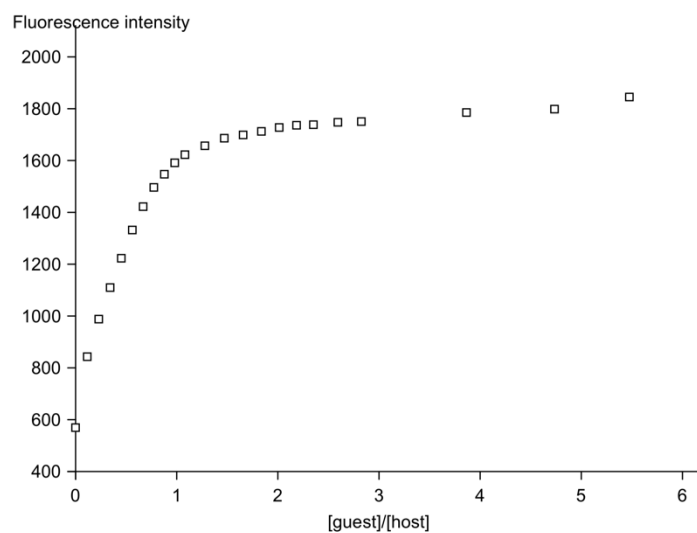


Figure S37 Changes in the emission intensity of [L2In(L')2] (8.9 μM) at 637 nm upon the addition of Sr(ClO4)2 (0–5.5 eq.) (CHCl3/EtOH = 9/1 (v/v), 293 K, $\lambda_{\text{ex}} = 400$ nm).

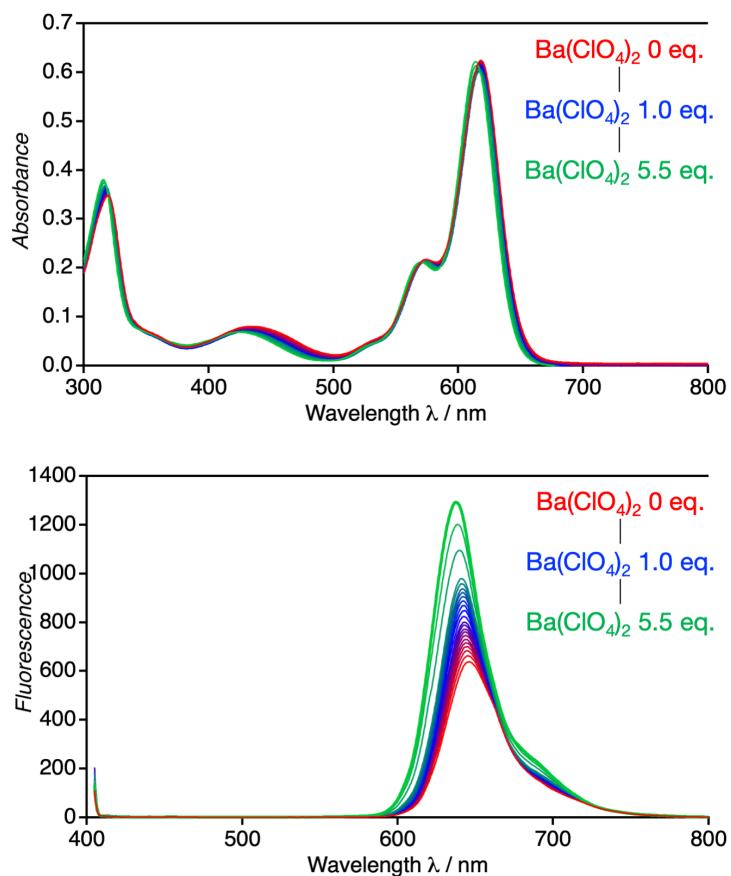


Figure S38 UV-vis absorption (top) and emission (bottom) spectral changes of [L2In(L')2] (L': solvent, 8.9 μM) upon the addition of Ba(ClO4)2 (0–5.5 eq.) (CHCl3/EtOH = 9/1 (v/v), 293 K, $\lambda_{\text{ex}} = 400$ nm).

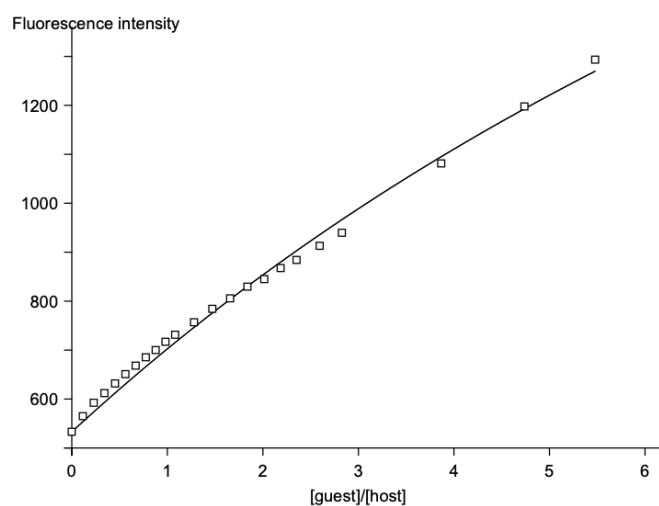


Figure S39 Changes in the emission intensity of [L2In(L')2] (8.9 μM) at 637 nm upon the addition of Ba(ClO4)2 (0–5.5 eq.) (CHCl3/EtOH = 9/1 (v/v), 293 K, $\lambda_{\text{ex}} = 400$ nm). The solid line shows the least squares fitting to determine the binding constant K_a (host:guest = 1:1, $\log K_a = 3.9 \pm 0.1$ ($\log(\text{M}^{-1})$))

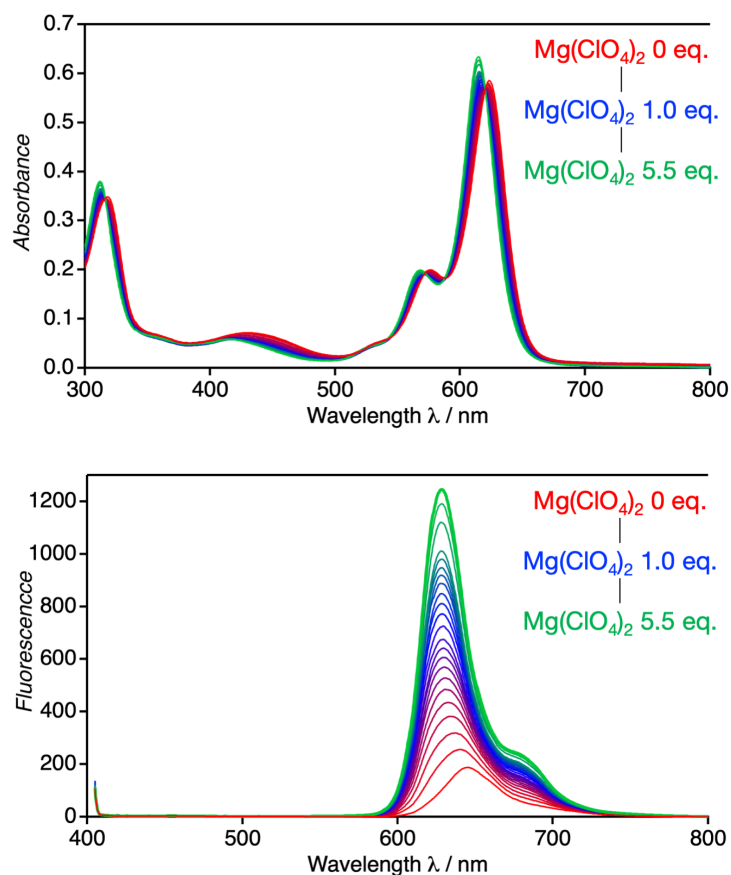


Figure S40 UV-vis absorption (top) and emission (bottom) spectral changes of $[\text{L}3\text{Al}(\text{L}')_2]$ (L' : solvent and/or pyridine, $8.9 \mu\text{M}$) upon the addition of $\text{Mg}(\text{ClO}_4)_2$ (0–5.5 eq.) ($\text{CHCl}_3/\text{EtOH} = 9/1$ (v/v), 293 K , $\lambda_{\text{ex}} = 400 \text{ nm}$).

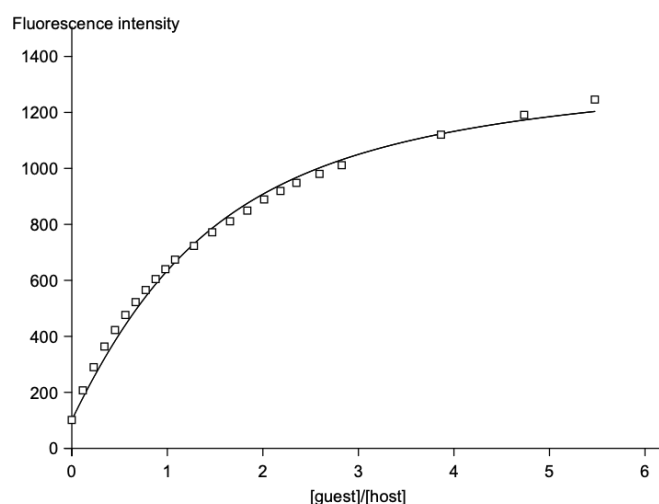


Figure S41 Changes in the emission intensity of $[\text{L}3\text{Al}(\text{L}')_2]$ ($8.9 \mu\text{M}$) at 628 nm upon the addition of $\text{Mg}(\text{ClO}_4)_2$ (0–5.5 eq.) ($\text{CHCl}_3/\text{EtOH} = 9/1$ (v/v), 293 K , $\lambda_{\text{ex}} = 400 \text{ nm}$). The solid line shows the least squares fitting to determine the binding constant K_a (host:guest = 1:1, $\log K_a = 5.12 \pm 0.04$ ($\log(\text{M}^{-1})$)).

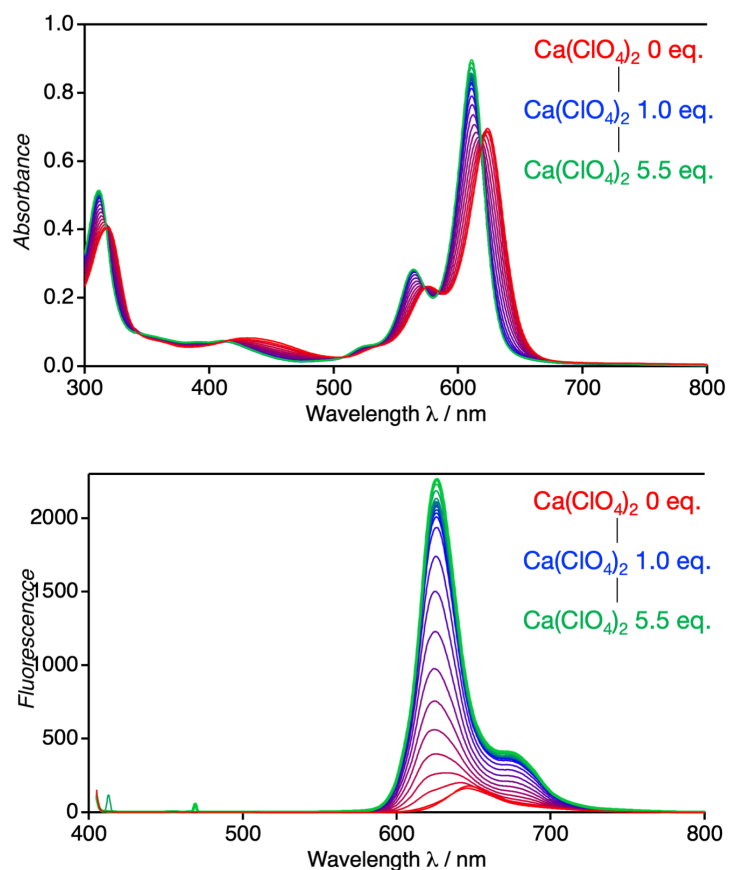


Figure S42 UV-vis absorption (top) and emission (bottom) spectral changes of $[\text{L3Al}(\text{L}')_2]$ (L' : solvent and/or pyridine, $8.9 \mu\text{M}$) upon the addition of $\text{Ca}(\text{ClO}_4)_2$ (0–4.4 eq.) ($\text{CHCl}_3/\text{EtOH} = 9/1$ (v/v), 293 K , $\lambda_{\text{ex}} = 400 \text{ nm}$).

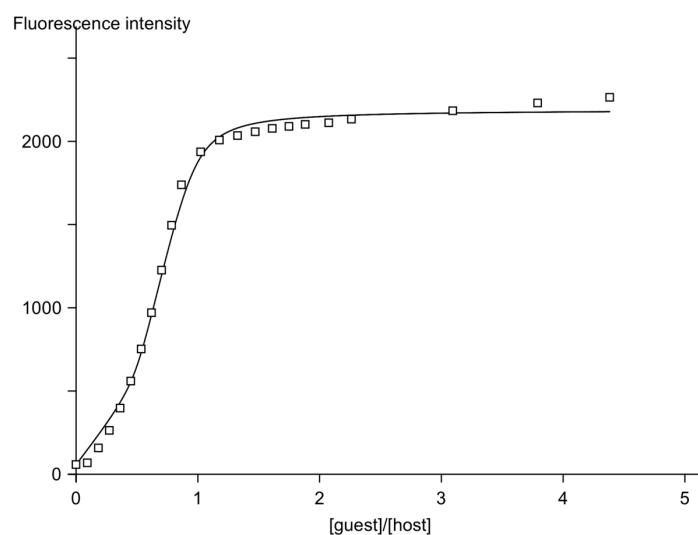


Figure S43 Changes in the emission intensity of $[\text{L3Al}(\text{L}')_2]$ ($8.9 \mu\text{M}$) at 626 nm upon the addition of $\text{Ca}(\text{ClO}_4)_2$ (0–4.4 eq.) ($\text{CHCl}_3/\text{EtOH} = 9/1$ (v/v), 293 K , $\lambda_{\text{ex}} = 400 \text{ nm}$). The solid line shows the least squares fitting to determine the binding constant K_a (host:guest = 2:1, $\log K_{a1} = 8.3 \pm 0.8$ ($\log(\text{M}^{-1})$), $K_{a2} = 6.5 \pm 0.9$ ($\log(\text{M}^{-1})$)).

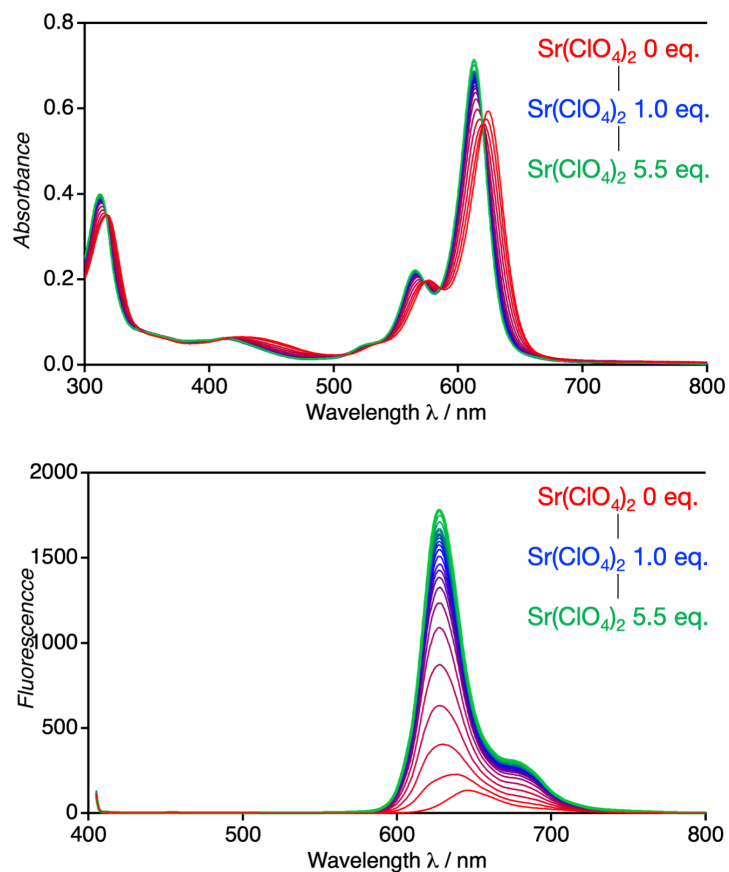


Figure S44 UV-vis absorption (top) and emission (bottom) spectral changes of $[\text{L}3\text{Al}(\text{L}')_2]$ (L' : solvent and/or pyridine, $8.9 \mu\text{M}$) upon the addition of $\text{Sr}(\text{ClO}_4)_2$ (0–5.5 eq.) ($\text{CHCl}_3/\text{EtOH} = 9/1$ (v/v), 293 K, $\lambda_{\text{ex}} = 400 \text{ nm}$).

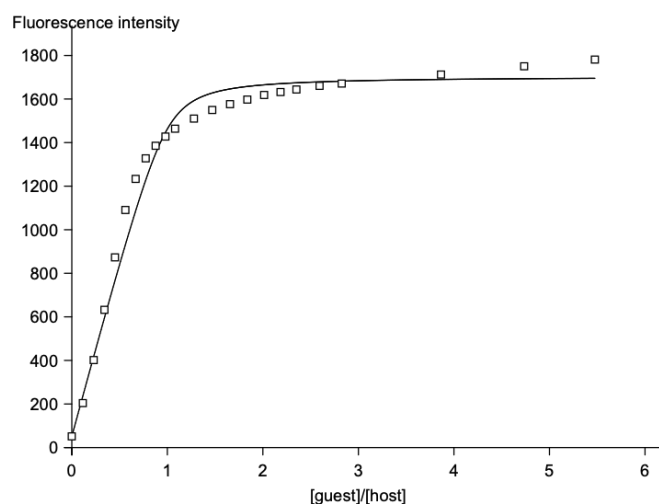


Figure S45 Changes in the emission intensity of $[\text{L}3\text{Al}(\text{L}')_2]$ ($8.9 \mu\text{M}$) at 627 nm upon the addition of $\text{Sr}(\text{ClO}_4)_2$ (0–5.5 eq.) ($\text{CHCl}_3/\text{EtOH} = 9/1$ (v/v), 293 K, $\lambda_{\text{ex}} = 400 \text{ nm}$). The solid line shows the least squares fitting to determine the binding constant K_a (host:guest = 1:1, $\log K_a = 6.7 \pm 0.2$ ($\log(\text{M}^{-1})$)).

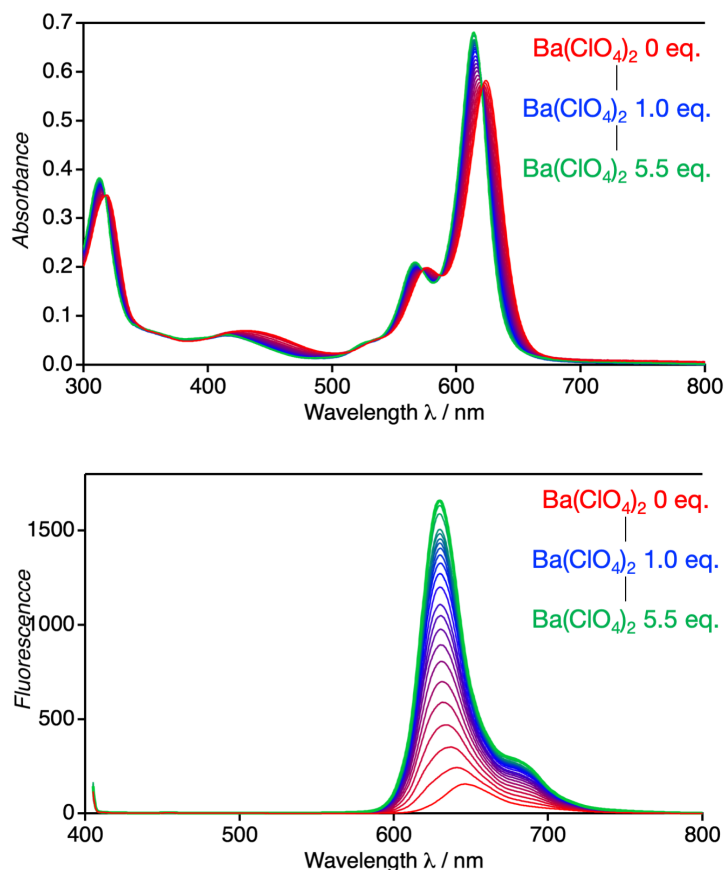


Figure S46 UV-vis absorption (top) and emission (bottom) spectral changes of $[\text{L3Al}(\text{L}')_2]$ (L' : solvent and/or pyridine, $8.9 \mu\text{M}$) upon the addition of $\text{Ba}(\text{ClO}_4)_2$ (0–5.5 eq.) ($\text{CHCl}_3/\text{EtOH} = 9/1$ (v/v), 293 K, $\lambda_{\text{ex}} = 400 \text{ nm}$).

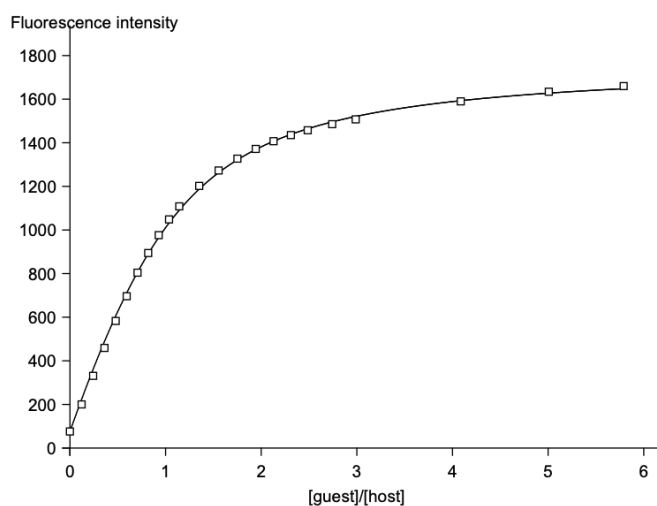


Figure S47 Changes in the emission intensity of $[\text{L3Al}(\text{L}')_2]$ ($8.9 \mu\text{M}$) at 630 nm upon the addition of $\text{Ba}(\text{ClO}_4)_2$ (0–5.5 eq.) ($\text{CHCl}_3/\text{EtOH} = 9/1$ (v/v), 293 K, $\lambda_{\text{ex}} = 400 \text{ nm}$). The solid line shows the least squares fitting to determine the binding constant K_a (host:guest = 1:1, $\log K_a = 5.50 \pm 0.02$ ($\log(\text{M}^{-1})$)).

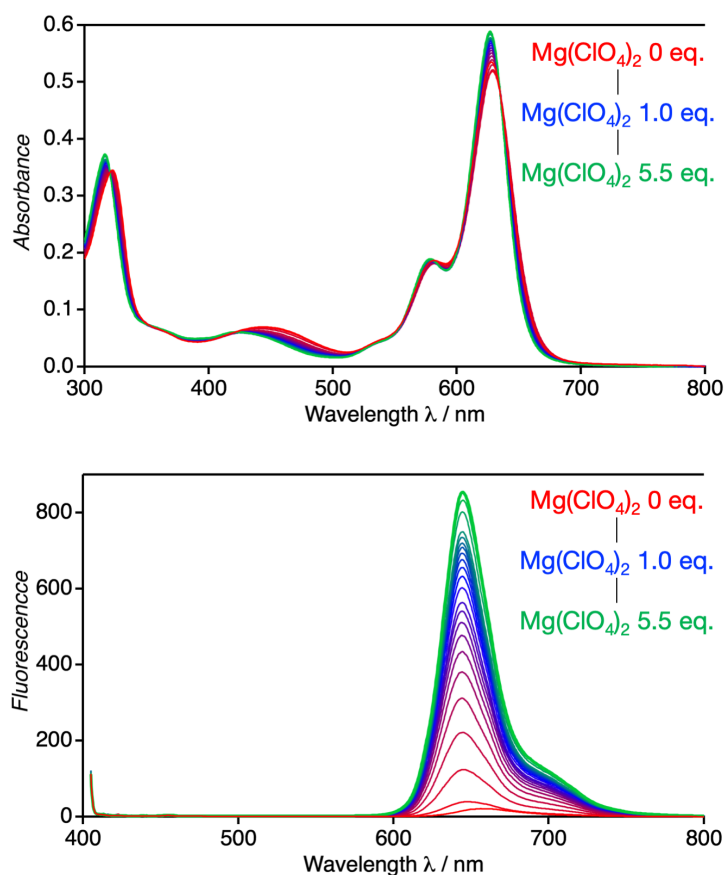


Figure S48 UV-vis absorption (top) and emission (bottom) spectral changes of $[\text{L3Ga}(\text{L}')_2]$ (L' : solvent and/or pyridine, $8.9 \mu\text{M}$) upon the addition of $\text{Mg}(\text{ClO}_4)_2$ (0–5.5 eq.) ($\text{CHCl}_3/\text{EtOH} = 9/1$ (v/v), 293 K , $\lambda_{\text{ex}} = 400 \text{ nm}$).

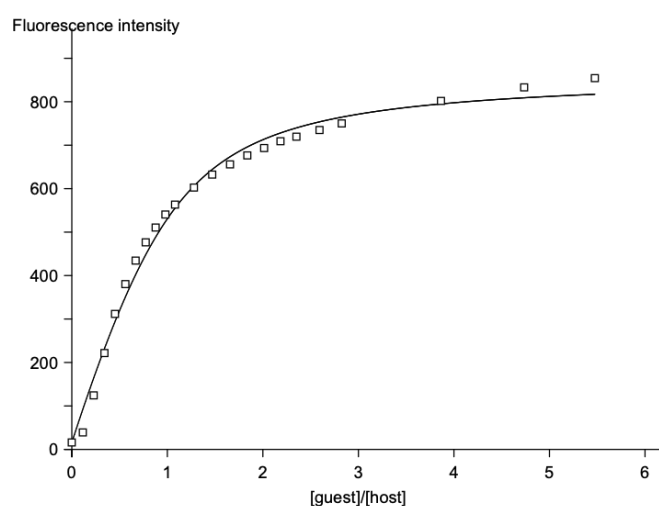


Figure S49 Changes in the emission intensity of $[\text{L3Ga}(\text{L}')_2]$ ($8.9 \mu\text{M}$) at 645 nm upon the addition of $\text{Mg}(\text{ClO}_4)_2$ (0–5.5 eq.) ($\text{CHCl}_3/\text{EtOH} = 9/1$ (v/v), 293 K , $\lambda_{\text{ex}} = 400 \text{ nm}$). The solid line shows the least squares fitting to determine the binding constant K_a (host:guest = 1:1, $\log K_a = 5.65 \pm 0.06$ ($\log(\text{M}^{-1})$)).

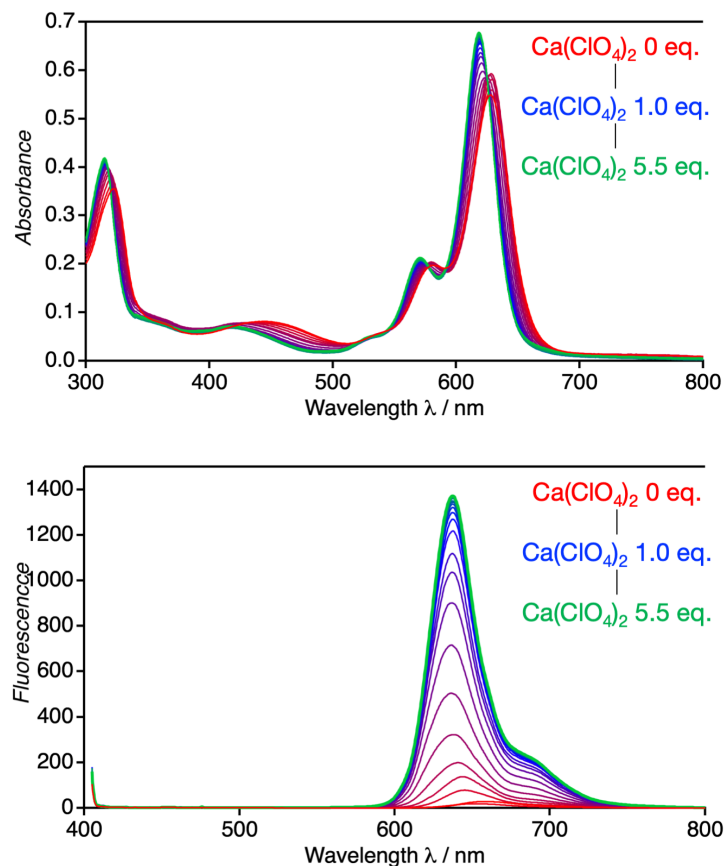


Figure S50 UV-vis absorption (top) and emission (bottom) spectral changes of $[\text{L3Ga}(\text{L}')_2]$ (L' : solvent and/or pyridine, $8.9 \mu\text{M}$) upon the addition of $\text{Ca}(\text{ClO}_4)_2$ (0–5.5 eq.) ($\text{CHCl}_3/\text{EtOH} = 9/1$ (v/v), 293 K, $\lambda_{\text{ex}} = 400 \text{ nm}$).

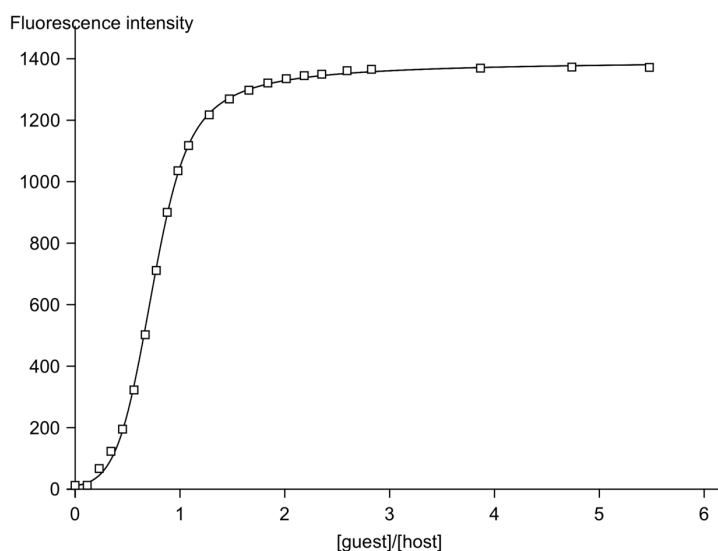


Figure S51 Changes in the emission intensity of $[\text{L3Ga}(\text{L}')_2]$ ($8.9 \mu\text{M}$) at 638 nm upon the addition of $\text{Ca}(\text{ClO}_4)_2$ (0–5.5 eq.) ($\text{CHCl}_3/\text{EtOH} = 9/1$ (v/v), 293 K, $\lambda_{\text{ex}} = 400 \text{ nm}$). The solid line shows the least squares fitting to determine the binding constant K_a (host:guest = 2:1, $\log K_{a1} = 7.5 \pm 0.1$ ($\log(\text{M}^{-1})$), $K_{a2} = 5.9 \pm 0.2$ ($\log(\text{M}^{-1})$)).

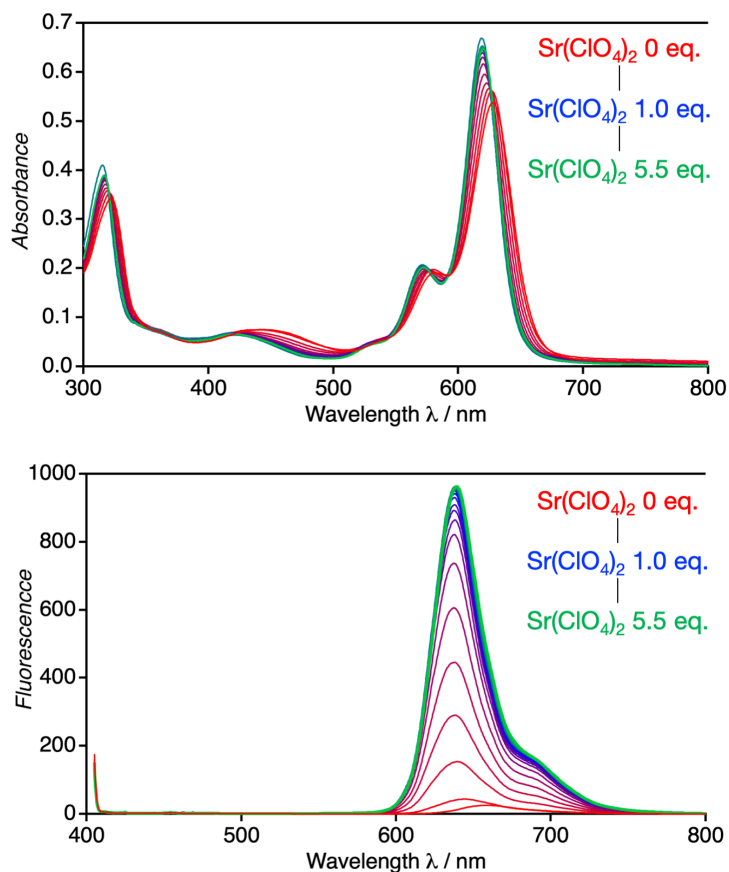


Figure S52 UV-vis absorption (top) and emission (bottom) spectral changes of [L3Ga(L')₂] (L': solvent and/or pyridine, 8.9 μM) upon the addition of Sr(ClO₄)₂ (0–5.5 eq.) (CHCl₃/EtOH = 9/1 (v/v), 293 K, λ_{ex} = 400 nm).

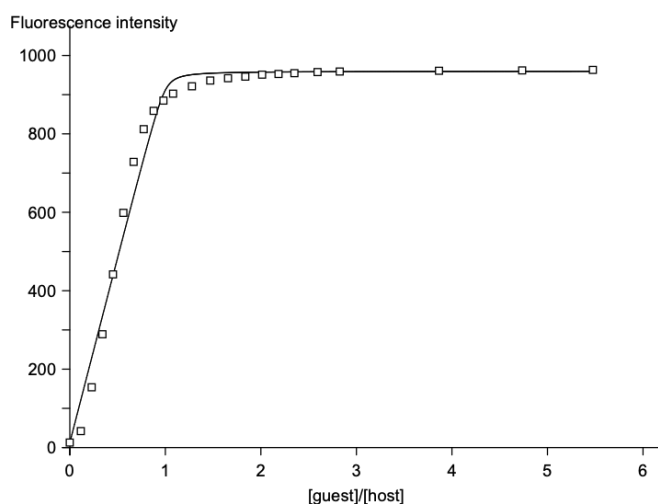


Figure S53 Changes in the emission intensity of [L3Ga(L')₂] (8.9 μM) at 639 nm upon the addition of Sr(ClO₄)₂ (0–5.5 eq.) (CHCl₃/EtOH = 9/1 (v/v), 293 K, λ_{ex} = 400 nm). The solid line shows the least squares fitting to determine the binding constant K_a (host:guest = 1:1, log $K_a = 7.6 \pm 0.6$ (log(M⁻¹)))

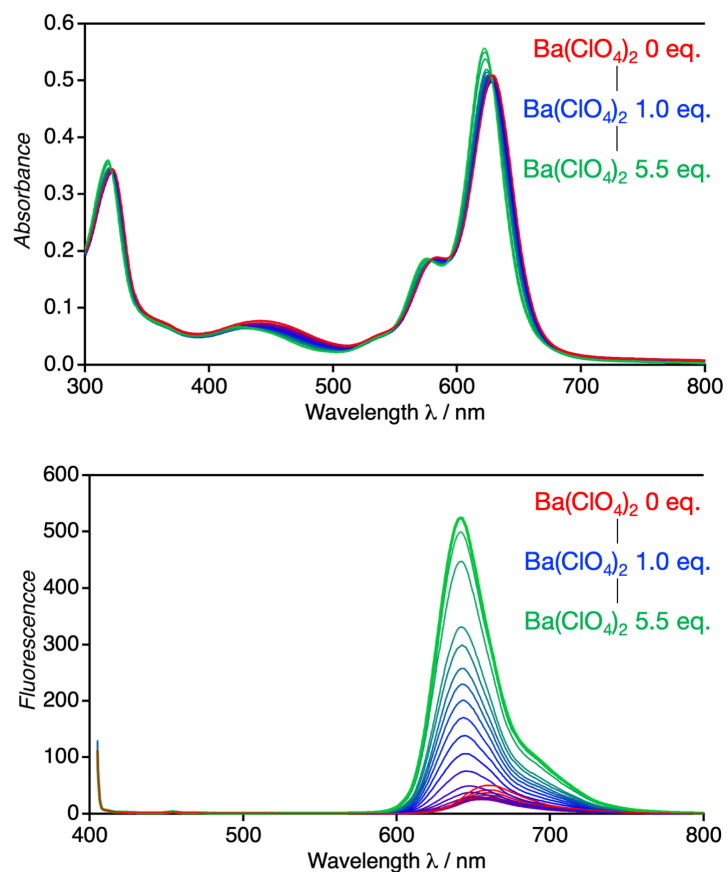


Figure S54 UV-vis absorption (top) and emission (bottom) spectral changes of $[\text{L3Ga}(\text{L}')_2]$ (L' : solvent and/or pyridine, $8.9 \mu\text{M}$) upon the addition of $\text{Ba}(\text{ClO}_4)_2$ (0–5.5 eq.) ($\text{CHCl}_3/\text{EtOH} = 9/1$ (v/v), 293 K , $\lambda_{\text{ex}} = 400 \text{ nm}$).

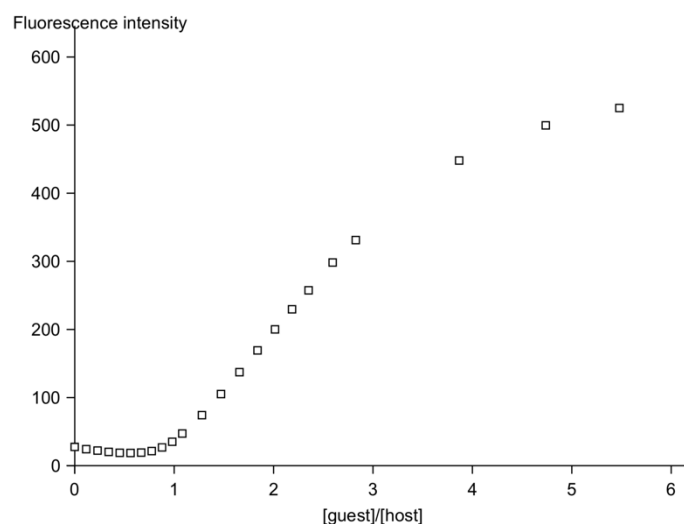


Figure S55 Changes in the emission intensity of $[\text{L3Ga}(\text{L}')_2]$ ($8.9 \mu\text{M}$) at 642 nm upon the addition of $\text{Ba}(\text{ClO}_4)_2$ (0–5.5 eq.) ($\text{CHCl}_3/\text{EtOH} = 9/1$ (v/v), 293 K , $\lambda_{\text{ex}} = 400 \text{ nm}$).

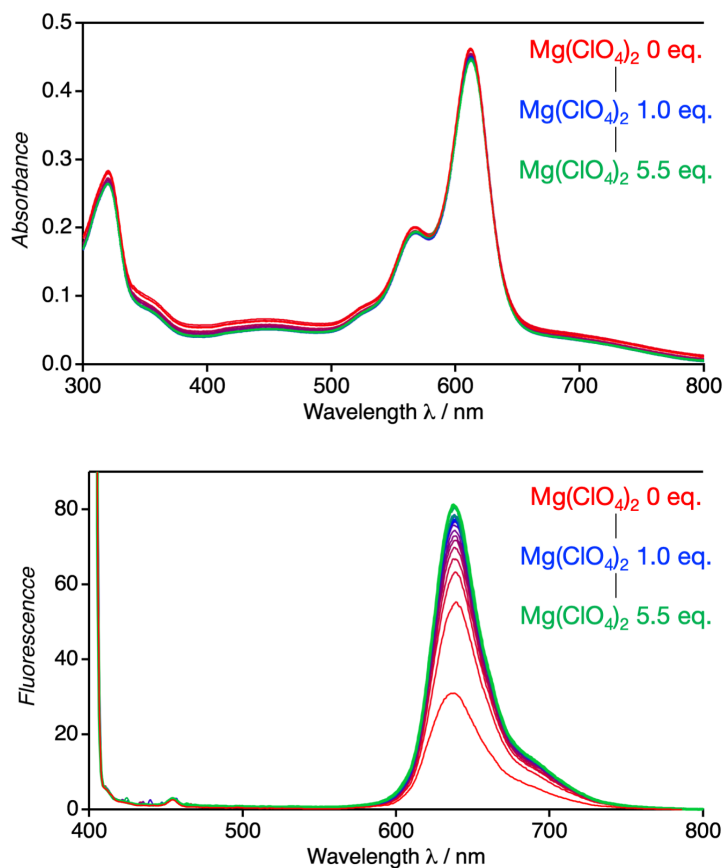


Figure S56 UV-vis absorption (top) and emission (bottom) spectral changes of $[\text{L}3\text{In}(\text{L}')_2]$ (L' : solvent, $8.9 \mu\text{M}$) upon the addition of $\text{Mg}(\text{ClO}_4)_2$ (0–5.5 eq.) ($\text{CHCl}_3/\text{EtOH} = 9/1$ (v/v), 293 K, $\lambda_{\text{ex}} = 400$ nm).

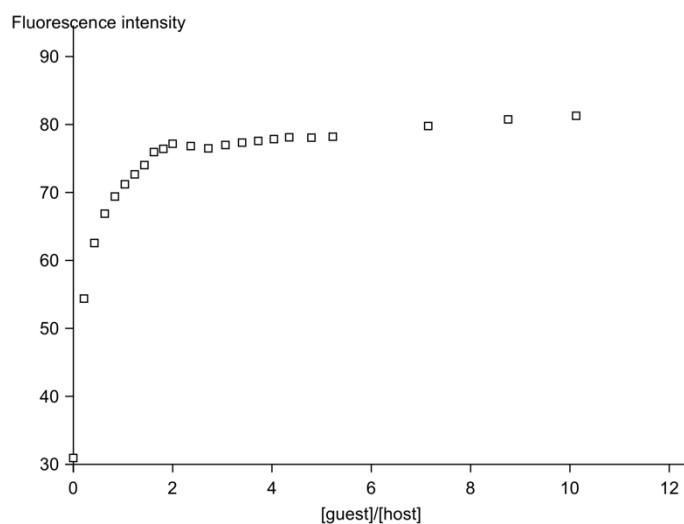


Figure S57 Changes in the emission intensity of $[\text{L}3\text{In}(\text{L}')_2]$ ($8.9 \mu\text{M}$) at 637 nm upon the addition of $\text{Mg}(\text{ClO}_4)_2$ (0–5.5 eq.) ($\text{CHCl}_3/\text{EtOH} = 9/1$ (v/v), 293 K, $\lambda_{\text{ex}} = 400$ nm).

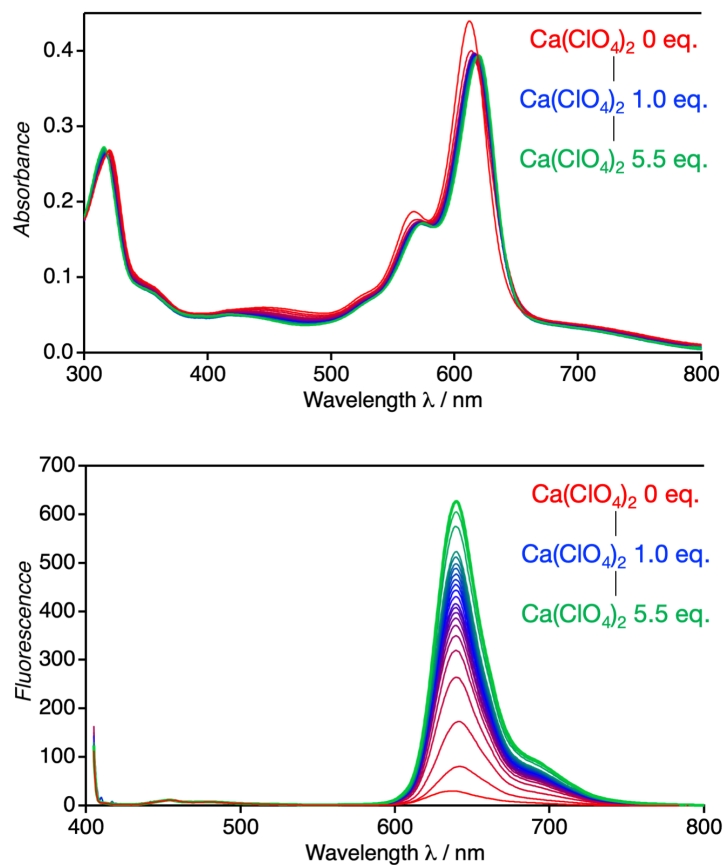


Figure S58 UV-vis absorption (top) and emission (bottom) spectral changes of $[\text{L3In}(\text{L}')_2]$ (L' : solvent, $8.9 \mu\text{M}$) upon the addition of $\text{Ca}(\text{ClO}_4)_2$ (0–5.5 eq.) ($\text{CHCl}_3/\text{EtOH} = 9/1$ (v/v), 293 K, $\lambda_{\text{ex}} = 400$ nm).

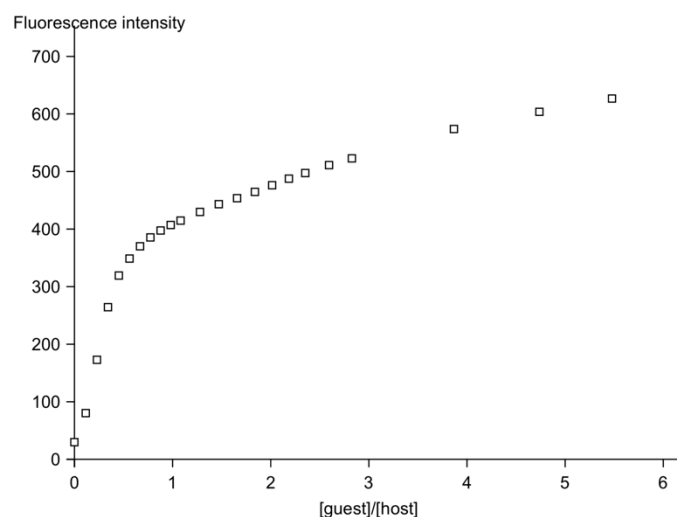


Figure S59 Changes in the emission intensity of $[\text{L3In}(\text{L}')_2]$ ($8.9 \mu\text{M}$) at 640 nm upon the addition of $\text{Ca}(\text{ClO}_4)_2$ (0–5.5 eq.) ($\text{CHCl}_3/\text{EtOH} = 9/1$ (v/v), 293 K, $\lambda_{\text{ex}} = 400$ nm).

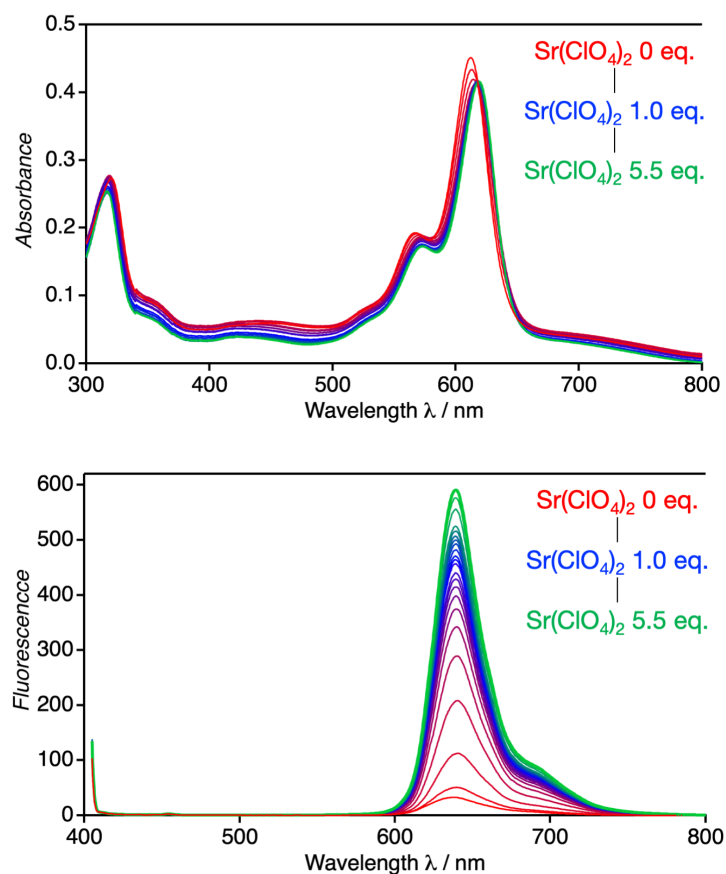


Figure S60 UV-vis absorption (top) and emission (bottom) spectral changes of [L3In(L')₂] (L': solvent, 8.9 μM) upon the addition of Sr(ClO₄)₂ (0–5.5 eq.) (CHCl₃/EtOH = 9/1 (v/v), 293 K, λ_{ex} = 400 nm).

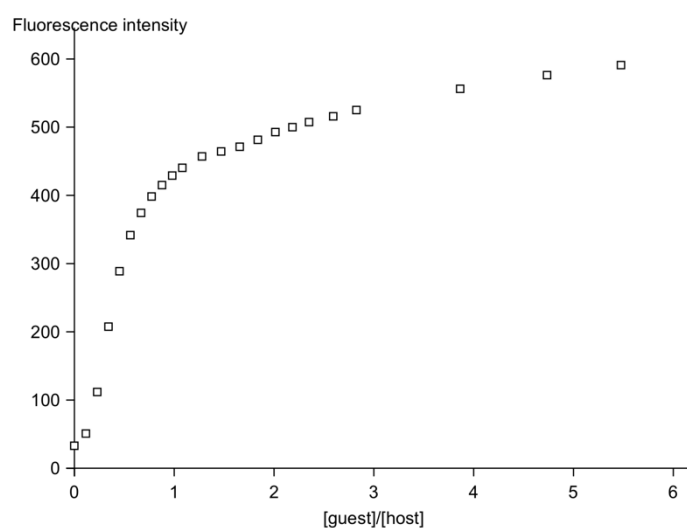


Figure S61 Changes in the emission intensity of [L3In(L')₂] (8.9 μM) at 639 nm upon the addition of Sr(ClO₄)₂ (0–5.5 eq.) (CHCl₃/EtOH = 9/1 (v/v), 293 K, λ_{ex} = 400 nm).

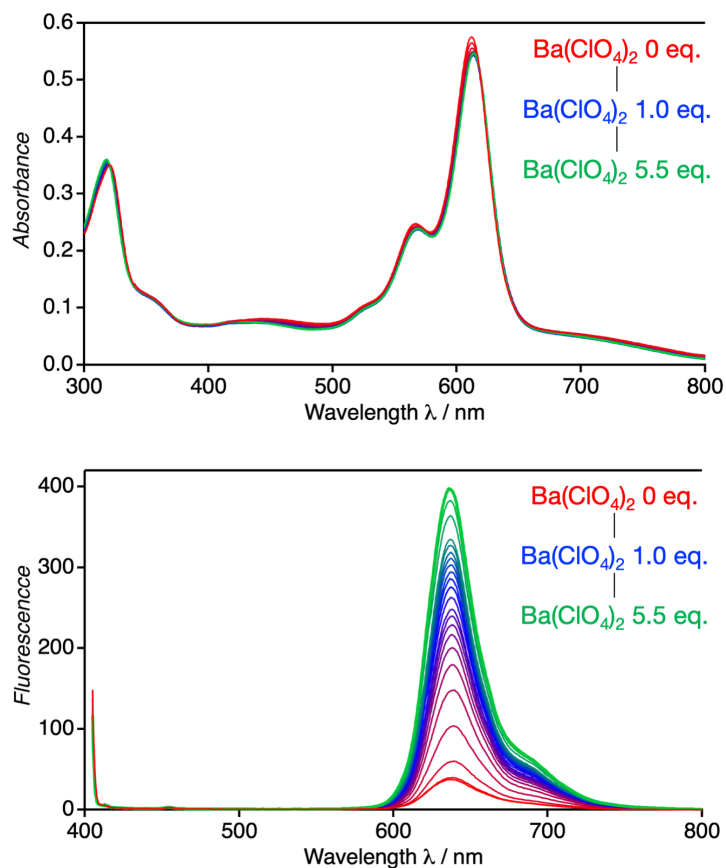


Figure S62 UV-vis absorption (top) and emission (bottom) spectral changes of [L3In(L')₂] (L': solvent, 8.9 μM) upon the addition of Ba(ClO₄)₂ (0–5.5 eq.) (CHCl₃/EtOH = 9/1 (v/v), 293 K, λ_{ex} = 400 nm).

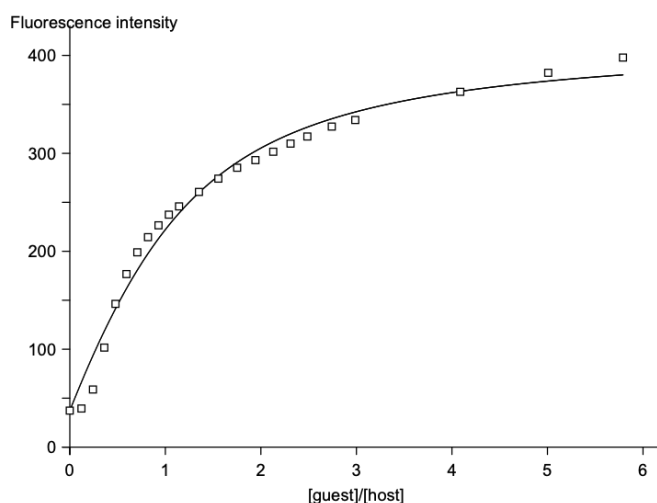


Figure S63 Changes in the emission intensity of [L3In(L')₂] (8.9 μM) at 636 nm upon the addition of Ba(ClO₄)₂ (0–5.5 eq.) (CHCl₃/EtOH = 9/1 (v/v), 293 K, λ_{ex} = 400 nm). The solid line shows the least squares fitting to determine the binding constant K_a (host:guest = 1:1, log $K_a = 5.31 \pm 0.07$ (log(M⁻¹)))

Table S1 Photoluminescence quantum efficiencies of the N₂O₄-type dipyrin complexes with alkaline earth ions (CHCl₃/EtOH = 9:1 (v/v), perchlorate salts, 298 K). 4.4 eq. (for the entry with an asterisk) or 5.5 eq. (for the others) of each ion was added.

	none	Mg ²⁺	Ca ²⁺	Sr ²⁺	Ba ²⁺
[L2In(L') ₂]	0.31	0.36	0.68	0.62	0.46
[L3Al(L') ₂]	0.055	0.30	0.41 *	0.31	0.34
[L3Ga(L') ₂]	0.009	0.31	0.49	0.34	0.11
[L3In(L') ₂]	0.006	0.008	0.33	0.24	0.15

X-ray crystallographic analyses

[L1Ga(py)]

A single crystal of [L1Ga(py)] suitable for X-ray diffraction analysis was obtained by slow evaporation of CHCl₃/pyridine solution of [L1Ga(L')₂].

Crystallographic data: C₇₀H₅₆GaN₆O₄, *F*w = 1184.65, purple block, 0.57 × 0.19 × 0.08 mm³, monoclinic, space group *P*2₁/*n*, *a* = 11.8153(7) Å, *b* = 17.1707(10) Å, *c* = 14.7240(8) Å, β = 110.951(2)°, *V* = 2789.7(3) Å³, *Z* = 4, *T* = 120(2) K, λ(MoKα) = 0.71073 Å, θ_{max} = 28.281°, *R*₁ = 0.0479, *wR*₂ = 0.1580, GOF = 1.002. CCDC No. 1915400.

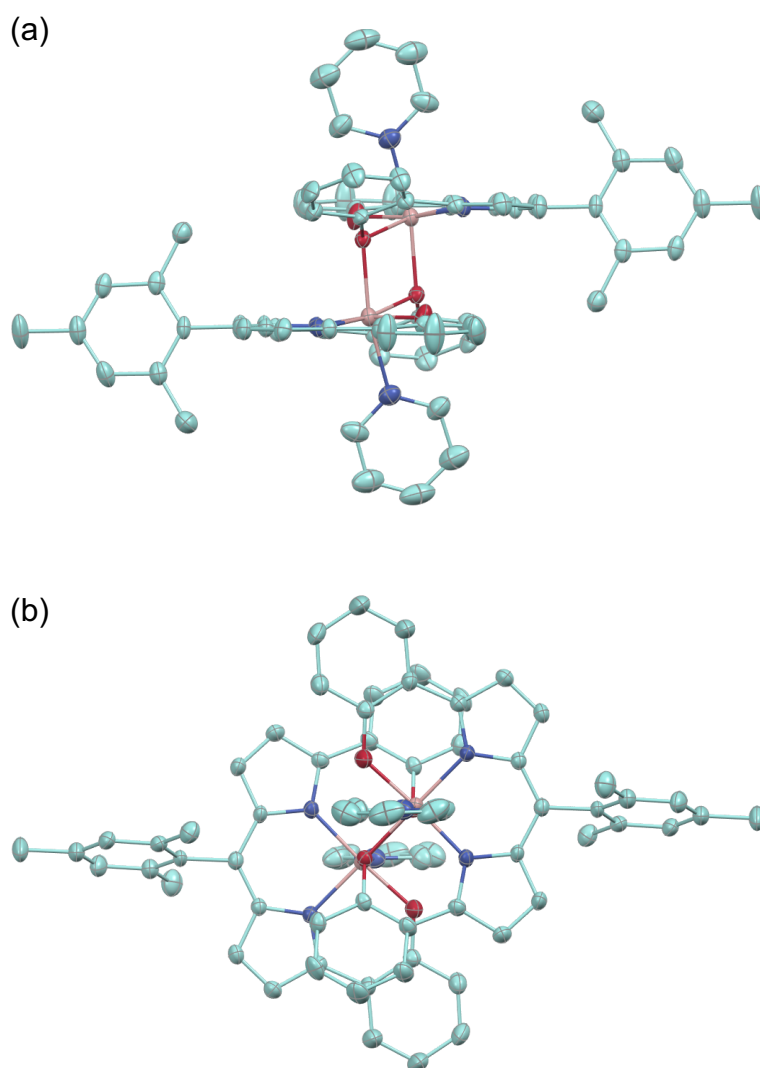


Figure S64 The molecular structure of the dimer of [L1Ga(py)] determined by X-ray crystallographic analysis: front view (a) and top view (b). An ellipsoidal model (50% probability). Hydrogen atoms are omitted for clarity. C, light green; N, blue; O, red; Ga, pink.

[L2In(H₂O)(CH₃OH)]

A single crystal of [L2In(H₂O)(CH₃OH)] suitable for X-ray diffraction analysis was obtained by vapor diffusion of pentane to CHCl₃/CH₃OH = 19/1 solution of [L2In(L')₂].

Crystallographic data: C_{102.5}H₁₁₁In₃N₆O₂₀, *F*w = 2091.43, blue plate, 0.17 × 0.16 × 0.05 mm³, triclinic, space group *P*-1, *a* = 13.5815(10) Å, *b* = 14.0146(10) Å, *c* = 25.346(2) Å, α = 80.911(2)°, β = 86.459(2)°, γ = 82.244(2)°, *V* = 4716.1(6) Å³, *Z* = 2, *T* = 120 K, λ(MoKα) = 0.71073 Å, θ_{max} = 26.372°, *R*₁ = 0.0604, *wR*₂ = 0.1393, GOF = 1.171. CCDC No. 1935885.

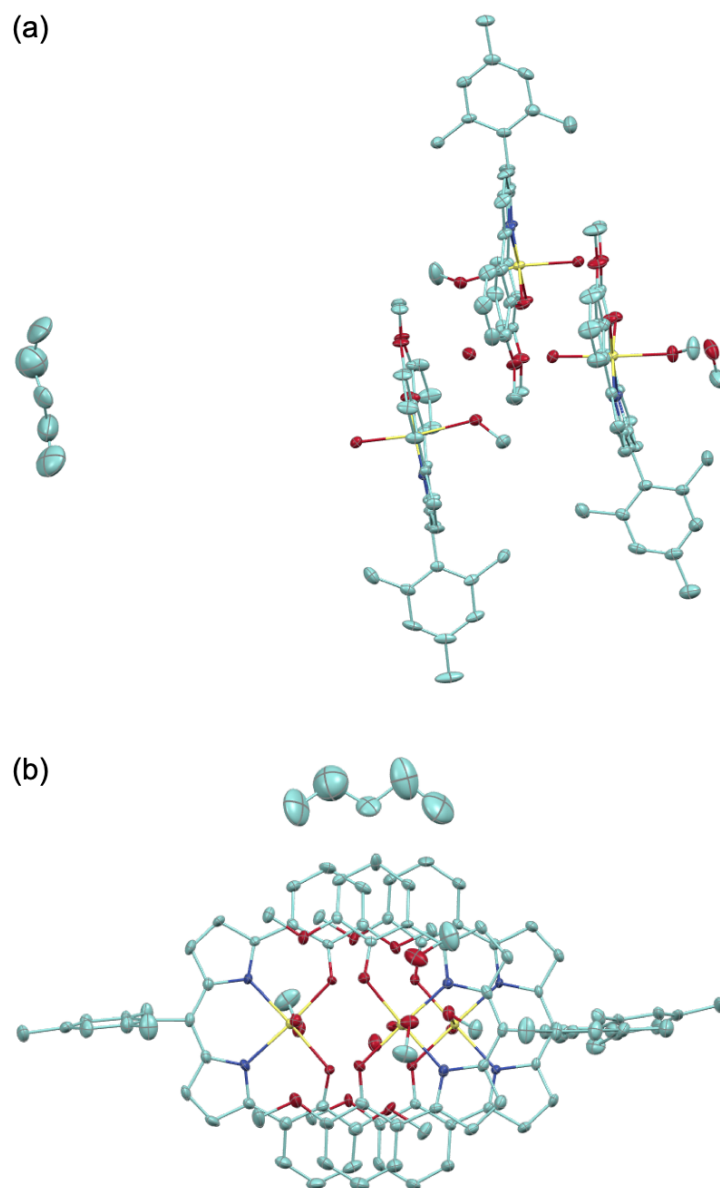


Figure S65 The molecular structure of [L2In(H₂O)(CH₃OH)] determined by X-ray crystallographic analysis: front view (a) and top view (b). Three non-equivalent molecules in an asymmetric unit are shown. An ellipsoidal model (50% probability). Hydrogen atoms are omitted for clarity. C, light green; N, blue; O, red; In, yellow.

[L3Ga(py)₂]

A single crystal of [L3Ga(py)₂] suitable for X-ray diffraction analysis was obtained by vapor diffusion of hexane to CHCl₃/pyridine = 1/1 solution of [L3Ga(L')₂].

Crystallographic data for L_{OH}Ga(py)₂: C₅₅H₄₈GaN₇O₄, *F*_w = 940.72, green plate, 0.010 × 0.13 × 0.29 mm³, monoclinic, space group *P*2₁/*n*, *a* = 9.4808(8) Å, *b* = 13.7142(12) Å, *c* = 35.759(3) Å, β = 94.458(2)°, *V* = 4635.4(7) Å³, *Z* = 4, *T* = 120 K, λ(MoKα) = 0.71073 Å, θ_{max} = 30.033°, *R*₁ = 0.0743, *wR*₂ = 0.1493, GOF = 1.191. CCDC No. 1915401.

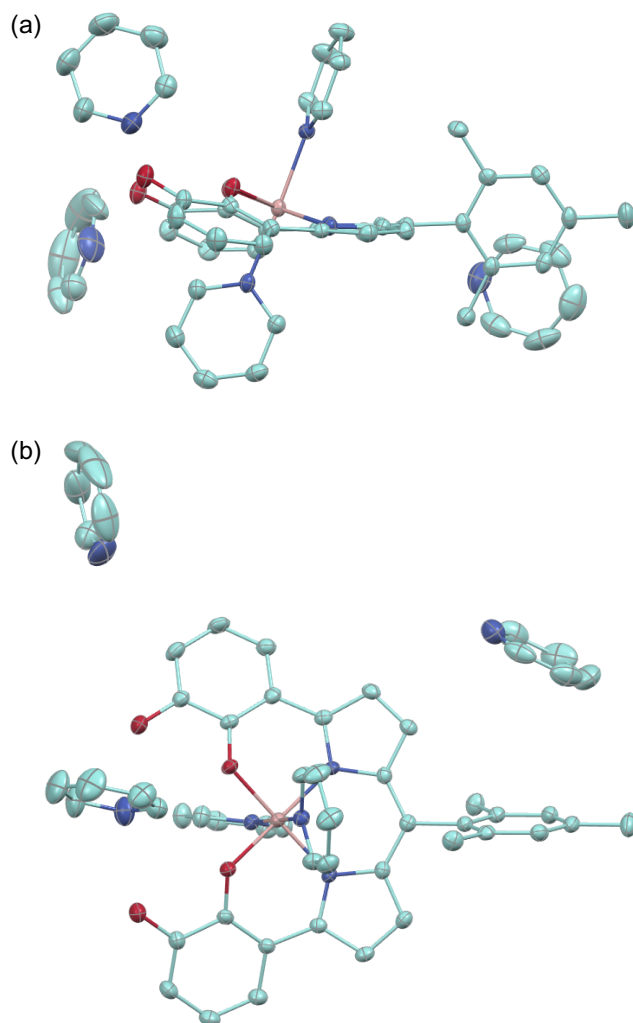


Figure S66 The molecular structure of [L3Ga(py)₂] determined by X-ray crystallographic analysis: front view (a) and top view (b). An ellipsoidal model (50% probability). Hydrogen atoms are omitted for clarity. C, light green; N, blue; O, red; Ga, pink.

References for the Supporting Information

- S1 K. Akine, *TitrationFit, ver 1.1.0, For analysis of titration data in host-guest chemistry*, 2013.